Chapter 5
Effect of Variables on Equilibrium Grain Boundary Segregation

There are many examples of both experimental and theoretical evidence of the effect of various thermodynamic and structural variables on the grain boundary segregation [20]. We did already see the complex effect of presence of several segregating elements (Chap. 4). Accepting its thermodynamic description in the sense of the thermodynamic approach [(4.32) and (4.33)], we can understand that the influence of individual parameters such as magnetic field, grain boundary structure and character of both segregating and matrix elements on grain boundary segregation is primarily involved in variations of the values of ΔH_I^0 and ΔS_I^0. Additionally, temperature affects the values of the whole exponential term in (4.32). Let us also mention that all the above-mentioned effects as well as pressure, and bulk and grain boundary concentrations contribute to variations of the values of ΔG_I^{E}. Among the intensive thermodynamic parameters affecting the segregation behaviour of individual systems, we can consider temperature, pressure, magnetic field and grain boundary energy. Grain size is an additional parameter affecting interfacial segregation.

5.1 Temperature and Bulk Composition

In a binary system, the value of the argument of the exponential term of segregation isotherm (4.32) approaches to negative infinity at low temperatures supposing $\Delta H_I^0 \neq 0$, and thus the exponent is equal to zero at $T = 0\,\mathrm{K}$. With increasing temperature, the absolute value of the exponent reduces causing that the grain boundary concentration decreases, as it is apparent from Fig. 5.1.

It is also seen from Fig. 5.1 that the course of this concentration decay depends on the values of both, the enthalpy and entropy of segregation, and the bulk concentration of the solute. Because practically the equilibrium is hardly reached at temperatures below 650 K, complete saturation of the boundary by the segregating element is not reached. In case of the solute with low absolute value of ΔH_I^0 (Fig. 5.1b), the equilibrium concentration at such temperatures is so low that we speak in such case about less segregating element although theoretically, it should completely cover the boundary at very low temperatures. In case of the element with

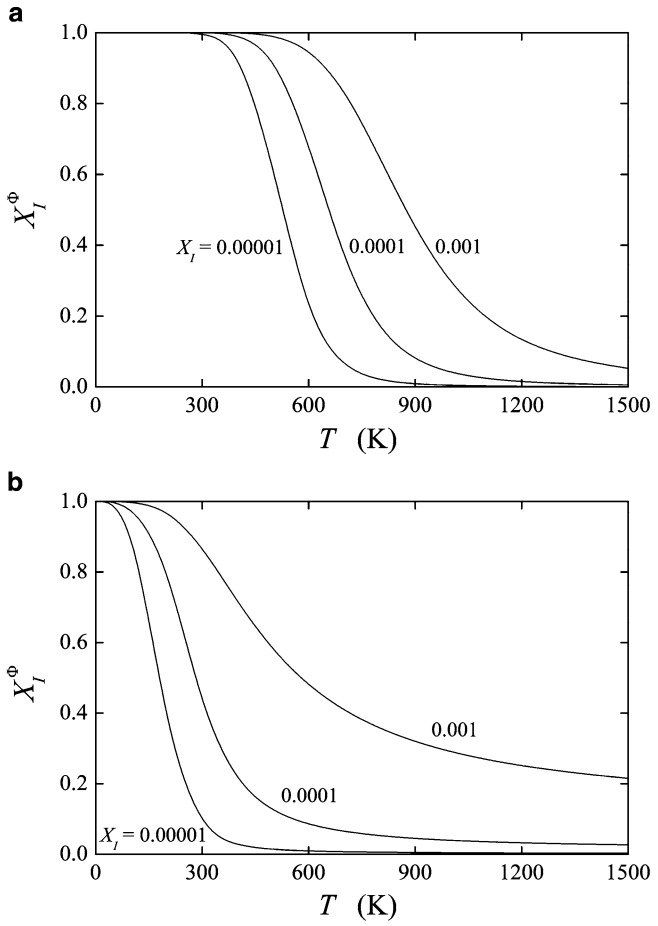

Fig. 5.1 Temperature dependence of grain boundary concentration in model binary systems characterised by (**a**) $\Delta H_I^0 = -50\,\text{kJ/mol}$, $\Delta S_I^0 = 0$, and (**b**) $\Delta H_I^0 = -10\,\text{kJ/mol}$, $\Delta S_I^0 = +40\,\text{J/(mol K)}$, for three different bulk concentration levels, 0.1, 0.01 and 0.001at.%

rather high absolute value of ΔH_I^0, the monolayer segregation can also be reached at real temperatures. It is also worth noting that solute segregation does not depend on the melting point: The segregation isotherm (cf. (4.32)) is identical for all elements and the melting temperature is not included there. Therefore, in the case of the matrix elements with low melting point (such as aluminium or indium), we may expect to observe large segregation effects just below the melting point, while in case of the matrix elements with high melting point, the segregation effects below the melting temperature are very weak.

In case of a multi-component alloy, the segregation behaviour depends on mutual interaction of the segregating elements. Assuming the segregation of the same

solutes in identical matrix as shown, for example in Fig. 5.1, we can distinguish principally four different cases:

(a) Non-interactive segregation on different sites
(b) Site competitive segregation at the same sites
(c) Segregation with repulsive interaction
(d) Segregation with attractive interaction

All these cases are documented in Figs. 5.2 and 5.3. It is apparent that the character of the temperature dependence of the grain boundary concentration is different in individual cases. In case of non-interactive segregation at different sites at the

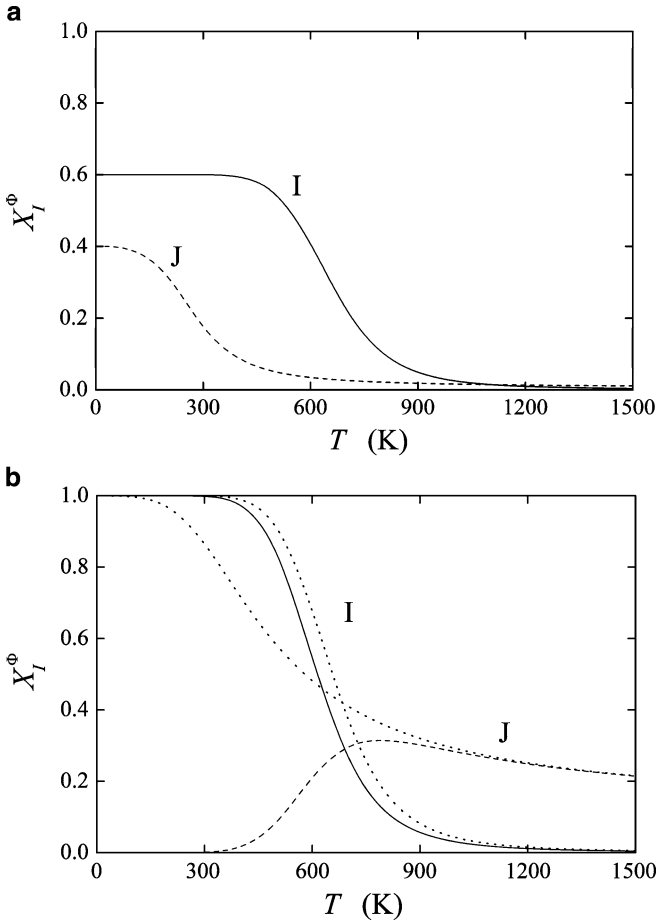

Fig. 5.2 Temperature dependence of the grain boundary concentration in model ternary systems characterised by $\Delta H_I^0 = -50\,\text{kJ/mol}$, $\Delta S_I^0 = 0$, $\Delta H_J^0 = -10\,\text{kJ/mol}$, $\Delta S_J^0 = +40\,\text{J/(mol K)}$, $X_I = 0.0001$, $X_J = 0.001$. (**a**) Non-interactive segregation to different sites ($X_I = 0.6$, $X_J = 0.4$); (**b**) site competitive segregation at identical sites. *Dotted lines* represent the behaviour of the solutes in binary alloys (cf. Fig. 5.1)

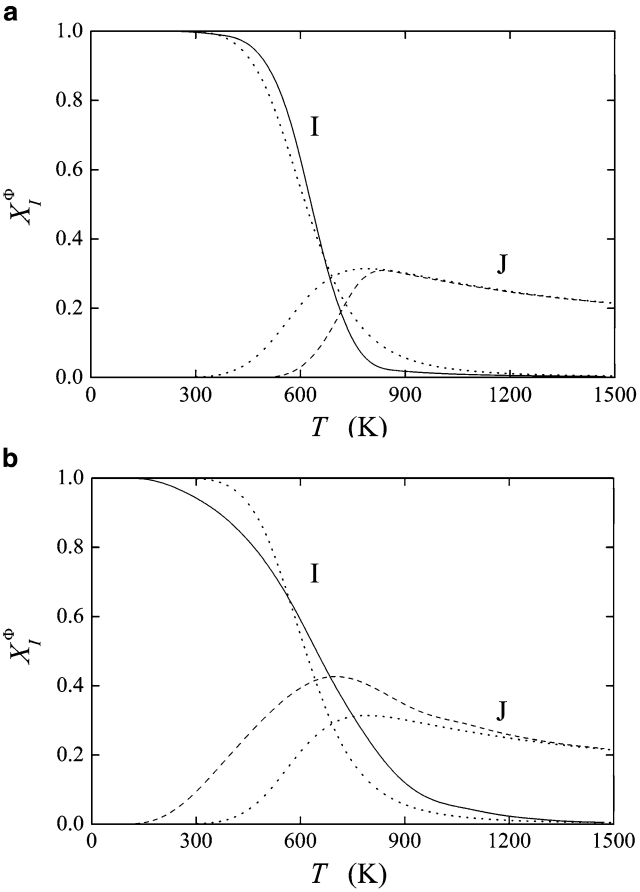

Fig. 5.3 Temperature dependence of the grain boundary concentration in model ternary systems characterised by $\Delta H_I^0 = -50$ kJ/mol, $\Delta S_I^0 = 0$, $\Delta H_J^0 = -10$ kJ/mol, $\Delta S_J^0 = +40$ J/(mol K), $X_I = 0.0001$, $X_J = 0.001$. (**a**) Segregation with repulsive interaction, $\alpha'_{IJ} = +20$ kJ/mol; (**b**) segregation with attractive interaction, $\alpha'_{IJ} = -20$ kJ/mol. *Dotted lines* represent the behaviour of the solutes in non-interacting ternary alloys (cf. Fig. 5.2b)

interface (Fig. 5.2a), the segregation of both elements is similar to that found for a binary system, that is independent of the grain boundary concentration of the other element. In this case, we speak about the segregation in a pseudobinary system. The only difference is that the grain boundary concentrations of both solutes do not approach 1 at 0 K, but they approach the doles of the sites of corresponding type at the interface.

When both solutes segregate at the same sites, a *site competition* occurs (cf. Chap. 4). At low temperatures, it is characterised by complete occupation of the interface by the solute I with a higher segregation tendency (higher $\left|\Delta H_I^0\right|$), while the less segregating solute J (lower $\left|\Delta H_J^0\right|$) is completely repelled from the grain

boundary. At higher temperatures, the concentration of J increases but it is still $X_J^{\Phi} < X_J$: this situation is understood as the grain boundary *depletion* from J. With increasing temperature, X_I^{Φ} decreases similarly as it does in the binary alloy (dotted line in Fig. 5.2b) and therefore, more grain boundary sites become available for segregation of J. X_J^{Φ} then increases with increasing T, reaches maximum and decreases thus approaching the concentrations comparable to its equilibrium value of the grain boundary segregation in a binary alloy (dotted line in Fig. 5.2b) at the same temperature. When the solutes interact with each other, the courses of the temperature dependence of their grain boundary concentrations change quantitatively depending on the character of the interaction (Fig. 5.3). In case of the repulsive interactions (Fig. 5.3a), the segregation of the more surface-active element I dominates at lower temperatures again but the decrease of its interfacial concentration at intermediate temperatures is more sharp than in a non-interacting system, that is the derivation of the temperature dependence in the inflection point is more negative under repulsive interaction. The absolute value of the slope of the temperature dependence of the grain boundary segregation of the more active solute increases with increasing value of the ternary interaction coefficient α'_{IJ} and at high values, it may cause an abrupt change from a very high concentration to a very low one. The segregation of the less surface-active element J is reduced due to repulsive interaction and is shifted to higher temperatures.

In case of the attractive interaction between segregating solutes, the more surface-active solute also possesses higher interfacial concentration, however, due to an attractive interaction, the less surface-active solute starts to segregate at much lower temperatures than in a non-interactive system. The slopes of the curves are much lower than in system with repulsive interaction as well as in non-interacting systems.

In fact, the repulsive interaction means that both elements repeal each other from the grain boundary, while in case of the attractive interaction both elements tend to segregate more strongly compared to the non-interactive case. It can be understood in terms of the grain boundary concentration of the matrix element: At a given temperature, its interfacial concentration is higher when both solutes mutually repeal, and lower when they attract (Fig. 5.4).

The character of the temperature dependence of the grain boundary segregation in a ternary alloy also changes with changing values of the thermodynamic parameters of interfacial segregation and the bulk concentration: Under some circumstances, a qualitative change of the temperature dependence of the grain boundary segregation may even occur (e.g. a dominating segregation of the solute with lower $\left|\Delta H_I^0\right|$ when its bulk concentration is large enough) [327].

5.2 Pressure

It follows from (4.49) and (4.51) that ΔG_I^0, ΔH_I^0 and ΔS_I^0 are *principally independent of pressure*. However, the studies – although only rarely described in literature – show a pronounced effect of pressure on interfacial segregation. Lee and Chiang

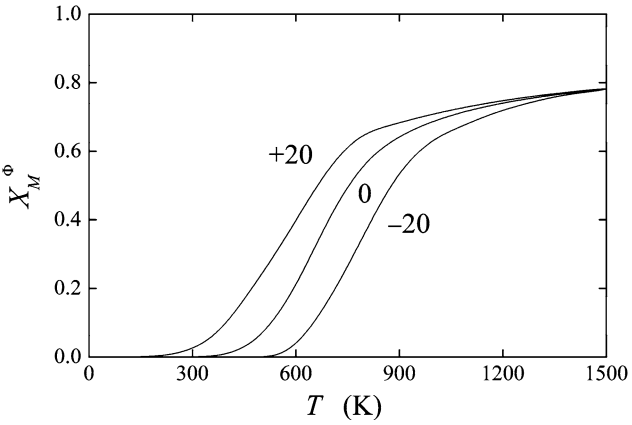

Fig. 5.4 Temperature dependence of the grain boundary concentration of the matrix element in model ternary systems characterised by $\Delta H_I^0 = -50\,\text{kJ/mol}$, $\Delta S_I^0 = 0$, $\Delta H_J^0 = -10\,\text{kJ/mol}$, $\Delta S_J^0 = +40\,\text{J/(mol K)}$, $X_I = 0.0001$, $X_J = 0.001$ and by the values of the ternary interaction parameter, $\alpha'_{IJ} = +20\,\text{kJ/mol}$, 0 and $-20\,\text{kJ/mol}$

found that the grain boundaries of ZnO are saturated by bismuth at ambient pressure (0.1 MPa) while its segregation at 1 GPa is completely suppressed [486]. Since ΔG_I^0 is independent of pressure, all changes in the chemical composition of grain boundaries are involved in the pressure dependence of the excess Gibbs energy of segregation,

$$\left(\frac{\partial \Delta G_I}{\partial P}\right)_{T,n_i} = \left(\frac{\partial \Delta G_I^{\text{E}}}{\partial P}\right)_{T,n_i} \tag{5.1}$$

and, thus, in the pressure dependence of corresponding activity coefficients. This effect is so high to reduce the Gibbs energy of segregation from $-65\,\text{kJ/mol}$ at 0.1 MPa to zero at 1 GPa.

This finding is in agreement with expectations that high pressure will prevent grain boundary segregation [487]. The reason for it might also be connected with the pressure effect on the phase diagrams by shifting the solvus-line, that is by increasing the solid solubility limit at a given temperature with increased pressure.

5.3 Magnetic Effects

Similarly to the effect of pressure, magnetism affects segregation behaviour of individual solutes. Here, we should recognise two effects (a) the effect of the magnetic state of the material and (b) the effect of external magnetic field on grain boundary segregation.

The Gibbs energy of segregation, ΔG_I, in (4.65) is characteristic for segregation in *paramagnetic* state. When the matrix is ferromagnetic, the total Gibbs energy of

segregation, ΔG_I^{T}, used in exponent of the segregation isotherm will additionally contain a ferromagnetic term ΔG_I^{F} [488],

$$\Delta G_I^{\mathrm{T}} = \Delta G_I + \Delta G_I^{\mathrm{F}}. \tag{5.2}$$

The ferromagnetic term ΔG_I^{F} is temperature dependent and can be approximated by

$$\Delta G_I^{\mathrm{F}}(T) = (1 - mX_I)\left(T_{\mathrm{c}}/T_{\mathrm{c}}^0\right)\Delta G_M^{\mathrm{F}}(T_r), \tag{5.3}$$

where ΔG_M^{F} is the ferromagnetic term of the Gibbs energy for ferromagnetic matrix element M, T_{c}^0 and T_{c} are the Curie temperatures of pure matrix M and M–I solid solution, T_r is the temperature term defined as $T_r = TT_{\mathrm{c}}^0/T_{\mathrm{c}}$. m is the factor representing the effect of the solute element I on the size of ferromagnetic term approximated by $m = 1$ for nonmagnetic solutes and $m = 0$ for magnetic solutes [488]. It follows from this treatment that

$$\Delta H_I^{\mathrm{F}}(T) = (1 - mX_I)\left(T_{\mathrm{c}}/T_{\mathrm{c}}^0\right)\Delta H_M^{\mathrm{F}}(T_r) \tag{5.4}$$

and

$$\Delta S_I^{\mathrm{F}}(T) = (1 - mX_I)\Delta S_M^{\mathrm{F}}(T_r), \tag{5.5}$$

where the meaning of the enthalpy, ΔH_M^{F}, and entropy, ΔS_M^{F}, corresponds to that of Gibbs energy, ΔG_M^{F}. It means in fact, that the dependence of G^{Φ} in ferromagnetic region of the concentration dependence of the Gibbs energy (Fig. 4.1) is shifted to higher values. The equilibrium concentration, X_I^{Φ}, corresponding to the parallel tangents of the shifted curve will also be higher as compared to the paramagnetic state. Detailed study of sulphur and antimony segregation in CoNi resulted in the values of $\Delta H_{\mathrm{Sb}}^0 = -5\,\mathrm{kJ/mol}$, $\Delta S_{\mathrm{Sb}}^0 = 38\,\mathrm{J/(mol\,K)}$, $\Delta S_{\mathrm{S}}^0 = -32\,\mathrm{kJ/mol}$ and $\Delta S_{\mathrm{S}}^0 = 47\,\mathrm{J/(mol\,K)}$ [488]. An analysis of the data on phosphorus segregation in bcc iron from the viewpoint of the magnetic effect provided us with the values of $\Delta H_{\mathrm{P}} = -15\,\mathrm{kJ/mol}$ and $\Delta S_{\mathrm{P}} = 33\,\mathrm{J/(mol\,K)}$ [488]. In fact, the correlation of experimental data on phosphorus grain boundary concentration [328] in the ferromagnetic region fully corresponds with that using the values of $\Delta H_{\mathrm{P}}^0 = -34.3\,\mathrm{kJ/mol}$ and $\Delta S_{\mathrm{P}}^0 = 21.5\,\mathrm{J/(mol\,K)}$ [328] but differs slightly in paramagnetic region. In fact, the data on solute segregation at grain boundaries given in Appendix A should be considered as corresponding to ferromagnetic state. Further conclusion about the effect of ferromagnetism is that it strengthens the segregation effects.

External magnetic field may affect the grain boundary segregation of both magnetic and surprisingly even non-magnetic materials. An increase of the grain boundary energy in the Fe–0.8at.%Sn alloy by 15 rel.% with increasing external magnetic field from 0 to 6 T was found during annealing the samples at 973 K [489, 490]. Based on findings of Seah and Hondros [307], it suggests that tin grain boundary concentration decreases with increasing effect of external magnetic field. This deduction was proved by direct measurement of grain boundary chemistry after

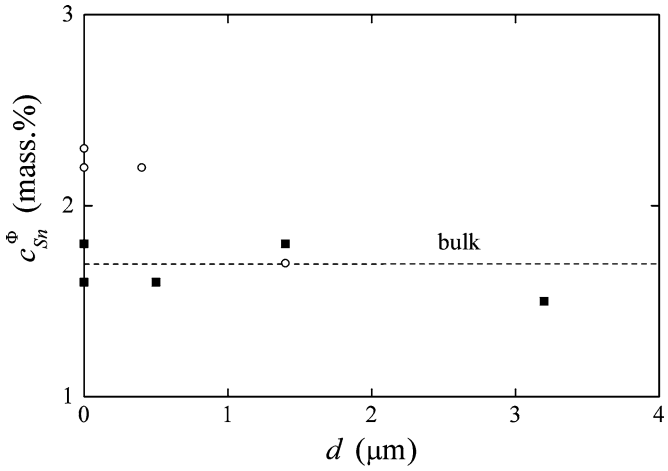

Fig. 5.5 Concentration of tin at grain boundaries of iron in depth d under the grain boundary after annealing at 973 K for 6 h without application of magnetic field (*empty circles*) and after annealing in magnetic field of 3 T (*solid squares*) (according to [490])

"magnetic annealing" at 973 K: While tin enrichment of the grain boundaries by factor 1.5 was found after annealing without application of magnetic field, no segregation was detected after annealing in magnetic field of 3 T [489] (Fig. 5.5). In fact, annealing of the samples in magnetic field is known for nearly 100 years as providing finer and more homogeneous structures of materials than conventional annealing without magnetic field [490].

Tsurekawa et al. [491] consider two sources for the effect of magnetic field on interfacial segregation (a) magnetic Gibbs energy and (b) grain boundary magnetism.

Magnetic Gibbs energy in ferromagnetic materials related to unit volume is generally given as [491]

$$\Delta G_I^{\mathrm{F}} = -\mu_0 \left(H - \frac{NM_{\mathrm{s}}}{2} \right) M_{\mathrm{s}}, \tag{5.6}$$

where μ_0 is the magnetic permeability of vacuum, M_{s} is the saturation magnetism, H is the strength of magnetic field and N is the demagnetising factor. In dia- and paramagnetic materials, the magnetic Gibbs energy per unit volume is

$$\Delta G_I^{\mathrm{D}} = \Delta G_I^{\mathrm{P}} = -\frac{1}{2}\mu_0 \chi (1 - \chi N) H^2, \tag{5.7}$$

where χ is the susceptibility. Paramagnetic tin atoms segregated at the grain boundaries of iron may be considered as "clouds," thus enhancing ΔG_I^{F} of the system in applied magnetic field despite the fact that these "clouds" do not affect the Curie temperature [492]. The reason for this enhancement is much higher magnetic

free energy of the system at the "cloud" than in the grain volume in magnetic field, that is $\Delta G_I^{\mathrm{P}} \gg \Delta G_I^{\mathrm{F}}$ due to extremely low susceptibility of tin (2.7×10^{-8} [491]). An estimate of the energy difference $\Delta G_I = \Delta G_I^{\mathrm{F}} - \Delta G_I^{\mathrm{P}}$ according to (5.6) and (5.7) assuming $N = 0$ gives $-6 \times 10^6\,\mathrm{J/m^3}$ for $H = 6\,\mathrm{T}$. Comparing this value with $\Delta G_{\mathrm{Sn}} = -6.5 \times 10^5\,\mathrm{J/m^3}$ reported by Seah and Lea for tin segregation in α-iron at 973 K [371], one can conclude that the magnetic Gibbs energy is one order of magnitude lower than the Gibbs energy of grain boundary segregation. As a consequence, application of a magnetic field will repeal tin atoms from the grain boundaries, because this process results in lowering the magnetic Gibbs energy and, thus, the Gibbs energy of the system [491]. It can also be assumed that the demagnetisation factor for the "cloud" depends on the direction of the magnetic field. It will be much lower for magnetic field being parallel to the grain boundary compared to the perpendicular case. Thus, the series $\Delta G_I^{\mathrm{P}}(\perp) > \Delta G_I^{\mathrm{P}}(||) \gg \Delta G_I^{\mathrm{F}}$ or $\Delta G_I^{\mathrm{D}}(\perp) > \Delta G_I^{\mathrm{P}}(||) \gg \Delta G_I^{\mathrm{F}}$ should be valid for segregated elements in paramagnetic state (e.g. tin) or diamagnetic state (e.g. copper), respectively.

Increased grain boundary magnetism is another possible explanation of the effect of magnetic field on grain boundary segregation. It was shown experimentally [493, 494] as well as theoretically [495] that the magnetic moment at the grain boundary is different from that of the grain volume and that it increases with decreasing atomic density. In case of tin in α-iron it can be well assumed that both the magnetisation and the Curie temperature are lower for segregated grain boundary than for the volume. Simultaneously, it can be expected that the difference in magnetisation of the grain boundary and the volume in a sample annealed at a temperature close to the Curie point will intensify the grain boundary segregation of tin. An external magnetic field will then evoke the field-induced magnetisation resulting in decrease of the difference in magnetisation of the grain boundary and the volume thus suppressing the grain boundary segregation caused by the magnetic effect [491].

5.4 Grain Boundary Energy

Changes in grain boundary energy affect the values of the chemical potentials of the solute and matrix elements at the grain boundary and thus the standard molar Gibbs energy of segregation (cf. Chap. 4, (4.30)). It results in *anisotropy of grain boundary segregation*.

Grain boundary energy exhibits a more-or-less pronounced dependence on the structure of the interface. Such dependence is shown, for example in Fig. 5.6. Due to the fact that grain boundary energy substantially contributes to the value of the chemical potentials (4.23) and according to the definition of thermodynamic quantities of grain boundary segregation as combination of chemical potentials (4.28) and (4.30), anisotropy of the thermodynamic quantities of grain boundary segregation must exist. Similarly, anisotropy of grain boundary composition may also

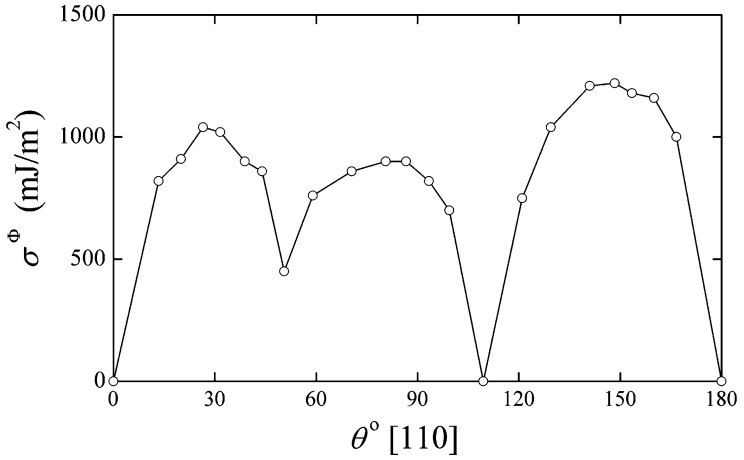

Fig. 5.6 Dependence of energy of symmetrical tilt grain boundaries, σ^{Φ}, on [110] misorientation angle θ in Ni–4at.%Pd alloy at 0 K (according to [341])

appear, however, due to its additional dependence on temperature, pressure and bulk composition of the alloy, it is not so straightforward as the anisotropy of the standard thermodynamic quantities.

Anisotropy of grain boundary segregation was experimentally detected for the first time from a scatter of data on chemical composition of individual "facets" on intergranular fracture surfaces, that is opened grain boundaries in polycrystalline materials albeit crystallographically unspecified. For example, variations of about ± 15 rel.% were found for tin and sulphur segregation in α-iron [307] and ± 45 rel.% for phosphorus segregation in a Cr–Mo low-alloy steel [173]. Grain boundaries in bismuth-doped copper were either fully decorated by bismuth or completely free of it [496]. Indications of non-homogeneous grain boundary segregation with scatters ranging from ± 30 to ± 60 rel.% were also reported in many other systems: for segregation of phosphorus [67, 166, 349, 497, 498], carbon [166, 430, 499], antimony [67, 419, 424, 500, 501], nickel [428, 500], manganese [67, 498], tin [500], molybdenum [426, 497], and chromium and oxygen [166, 428] in α-iron, and ferrite-based iron alloys and steels. Other examples are grain boundary segregation of antimony, sulphur and phosphorus in nickel [374, 454], of boron in Ni_3Al [502], of phosphorus in tungsten [370] or of iron in magnesia [192]. Generally, the majority of the literature data are confined in a broad region limited by the Maxwell distribution with scatter ± 60 rel.% for 50% of the Maxwell curve [20].

Experimental data on chemistry of a single grain boundary measured by methods of surface analysis on fracture surfaces can exhibit a scatter. This scatter up to about ± 10 rel.% can be caused by deviations of the fracture path from the interface, inhomogeneities of bulk chemical composition and lack of equilibrium. A larger scatter then reflects anisotropy of grain boundary segregation [67, 503]. Theoretical analysis of the bond strength suggests that intergranular fracture passes through a metallic

material by breaking the weakened metal–metal bonds in the neighbourhood of the strong metal–metalloid bonds [503–505]. The fracture path zigzags along the boundary and the segregated species are distributed between the two newly created fracture surfaces. It is usually supposed that this distribution is homogeneous, that is that on average, there is always one-half of the amounts of the segregated element(s) on each fracture surface. Some measurements of grain boundary composition on both matching fracture surfaces support this idea, e.g. phosphorus concentration on fracture surfaces of polycrystalline tungsten [372], Cr–Ni ferrite steel [67] and α-iron [343, 354]. Careful studies of composition of both matching fracture surfaces of well-characterised single grain boundaries in bicrystals brought progress in understanding this distribution. Markedly different phosphorus concentrations were found on both sides of a separated symmetrical {013} tilt grain boundary in a Fe–Si alloy [139]. Model calculations suggested that the fracture did not zigzag through the grain boundary core but passed parallel to the grain boundary at a distance of one atomic layer from the core over a relatively large area. After meeting, a defect at the grain boundary such as deformation twin occurring in front of the crack during breaking the bicrystal, the fracture can jump onto the corresponding path on the other side of this boundary. However, once the equilibrium grain boundary segregation is established, the fracture runs just in the grain boundary core and distributes the segregated species homogeneously to both fracture surfaces in the case of this grain boundary and in the case of other symmetrical interfaces [111]. On the other hand, systematic differences of composition between the two fracture surfaces found for asymmetrical grain boundaries suggest that fracture unevenly distributes the segregated species between the fracture surfaces [111]. The difference between chemical composition of both fracture surfaces can reach as much as ±30 rel.% [94, 506, 507].

Li and Williams [508] studied phosphorus segregation at individual grain boundaries in rapidly solidified Fe–0.6mass%P alloy. Despite a strong non-equilibrium character of such interfaces, they found heterogeneous distribution of phosphorus at the grain boundaries ranging from 0.05 to 0.4 monolayer with significantly lower segregation level at low-angle and low-Σ grain boundaries comparing to high-angle and high-Σ ones. During this AEM study, different phosphorus concentrations were detected on matching planes of the grain boundary.

To elucidate the relationship between the structure and chemical composition of individual grain boundaries, the measurements of interfacial segregation should be performed on well-characterised grain boundaries in bicrystals. Numerous experiments of this kind were performed in the past decades. Very low segregation has usually been observed at coherent twin grain boundaries, for example in case of copper in lead [509], phosphorus in an Fe–Si alloy [134, 510], bismuth in copper [511] and silicon and titanium in alumina [512]. It is worth noting that coherent twin boundaries are often found free of segregation [511]. Other grain boundaries exhibit higher or lower levels of segregation. Lower segregation was measured for antimony at 15°[110] and 100°[110] symmetrical tilt grain boundaries of copper than at 54°[110] and 67°[110] ones. Highly coincident grain boundaries did not show any segregation of antimony. Variation of antimony concentration along facetted

grain boundaries indicates that grain boundary plane orientation plays an important role in impurity segregation [511]. This conclusion is supported by the finding of weak silicon and titanium segregation at grain boundaries parallel to at least one dense lattice plane of alumina such as (0001) [512]. Three times higher sulphur concentration was detected at the 20°[100] tilt grain boundary in nickel as compared to the 40°[100] one [513]. Low levels of carbon and oxygen segregation were detected at the 5°[100] low-angle grain boundary in tungsten than at the 50°[100] and 48°[110] high-angle grain boundaries [514]. These findings may suggest that the tendency to grain boundary segregation increases with increasing misorientation angle of the two adjoining grains. Slightly higher segregation of calcium and silicon was detected at the $\Sigma = 17, 28.5°$[001] twist grain boundary in magnesia than at the $\Sigma = 5, 36.9°$[001] one: much higher levels of segregation were detected at general grain boundaries [515]. In Mn–Zn ferrites, low calcium segregation was detected at highly coincident grain boundaries such as $\Sigma = 13, \{015\}$ and asymmetrical grain boundaries having one of the boundary planes close to a low-index one, for example (110) and (111) in comparison to low-coincidence grain boundaries. Segregation of calcium was accompanied by a depletion of Fe^{2+} ions relatively to Fe^{3+} ions [516]. Similarly, highly coincident [100] grain boundaries ($\Sigma = 3, 5$ and 13) in tetragonal $YBa_2Cu_3O_{7-\delta}$ structure were found free of segregation while general grain boundaries often contained vitreous phase indicating strong segregation effects [517]. Low-angle [518] and low-Σ [519, 520] grain boundaries in $YBa_2Cu_3O_{7-\delta}$ exhibit identical composition as the grain interior. On the other hand, molybdenum, zirconium and strontium were found to segregate at less coincident grain boundaries [518].

Grain boundary structure also seems to have an effect on character of segregation in multi-component alloys. For example, silicon was found to segregate at both, $\Sigma = 9$, (011) twist grain boundary [241] and $\Sigma = 9$, [011] tilt grain boundary [521], whereas boron segregates at general grain boundaries in an Fe–Si alloy [240,521]. In both cases, carbon segregation at the same level was measured at the grain boundary fracture surfaces [240, 521], however, it is not clear whether its presence is due to segregation or surface contamination. A comparison of solute segregation at tilt and twist interfaces showed larger absorptive capacity of twist interfaces [522, 523].

Grain boundary concentration of a solute is affected by many factors discussed above, such as temperature, bulk concentration of segregating element and presence of other components in the system. For general description, the values of the enthalpy and entropy of segregation are necessary. There are several attempts to evaluate the values of the thermodynamic functions of segregation for individual grain boundaries. Surprisingly high values of ΔH_I were determined for niobium and iron segregation to stacking faults (i.e. twin grain boundary) in cobalt, $\Delta H_{Nb} = -60$ kJ/mol, $\Delta H_{Fe} = -30$ kJ/mol [522, 523]. This may result from inadequate application of the regular solution model to evaluate the thermodynamic data, because the driving force for segregation originates from third nearest neighbours and higher interactions [523]. The values $\Delta H^0_{In} = -38$ kJ/mol and $\Delta S^0_{In} = -0.05$ J/(mol K), and $\Delta H^0_{In} = -39$ kJ/mol and $\Delta S^0_{In} = -0.05$ J/(mol K) were determined for indium segregation at {115} and {1 1 10} grain boundaries of nickel, respectively,

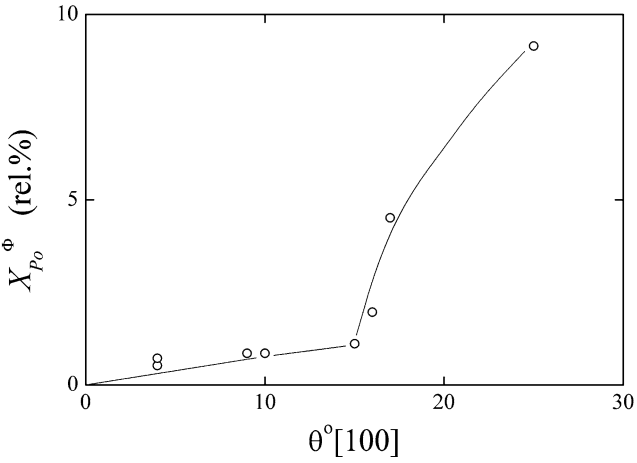

Fig. 5.7 Dependence of relative concentration of polonium at [100] symmetrical tilt grain boundaries of lead [525]

using the Langmuir–McLean segregation isotherm (4.61) [524]. Since the entropy term has only a very small effect on ΔG^0_{In}, we may accept $\Delta G^0_{\mathrm{In}} \approx \Delta H^0_{\mathrm{In}}$. The value $\Delta G^0_{\mathrm{In}} \approx -40\,\mathrm{kJ/mol}$ is lower than $-50\,\mathrm{kJ/mol}$ measured for general grain boundaries in polycrystalline material. Thus, the above mentioned well-characterised grain boundaries cannot be considered as general [524] but rather as vicinal.

To disclose characteristic differences in behaviour of individual interfaces, the detail systematic measurements of orientation dependence of solute segregation on a set of grain boundaries is necessary. Due to large variety of grain boundaries (5 DOFs, cf. Chap. 2), such systematic study is very complicated. Usually, a cut of the 6-dimensional space is used, where only one DOF is changing or that cut is well characterised. The dependence of solute segregation on the misorientation angle θ for symmetrical tilt grain boundaries can serve, for example of the last-mentioned case [20]. The first systematic study of structural dependence of this type was reported for polonium segregation at [100] symmetrical tilt grain boundaries of lead by autoradiography [525]. It showed an increase of grain boundary segregation with increasing misorientation angle. An abrupt rise of polonium concentration appears for grain boundaries above $\theta = 15°$ (Fig. 5.7). This change of the slope of the orientation dependence is very probably caused by the change of the grain boundary structure from low-angle dislocation one to that formed by structural units in case of the high-angle grain boundaries.

The dependence of the Auger peak-to-peak heights ratios r_I (which is a measure of the grain boundary concentration) on the misorientation angle of tilt grain boundaries without specifying the other DOFs was constructed for tin and silicon grain boundary segregation in bcc iron [526, 527] (Fig. 5.8). The data were fitted by a monotonic dependence (full lines in Fig. 5.8) and concluded that no increase of silicon concentration exists for low-angle grain boundaries $\theta < 15°$, while a very

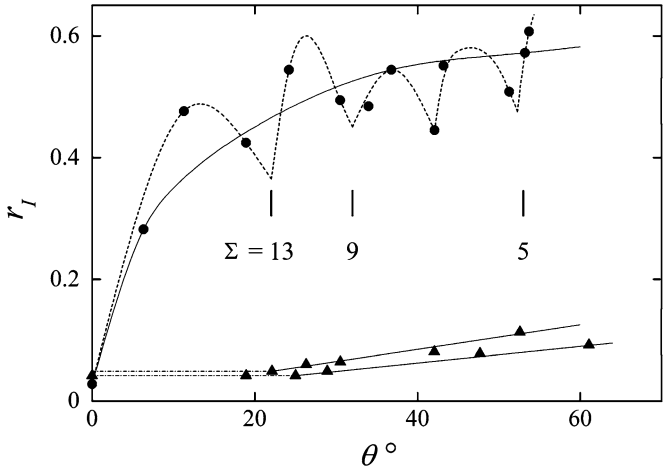

Fig. 5.8 Dependence of relative Auger peak-to-peak height ratios, r_I, of silicon (*triangles*) [527] and tin (*circles*) [526] on tilt angle of rotation as presented by Watanabe et al. (*full lines*). *Dotted line* shows an alternative interpretation of the data taking into account possible low segregation at special (highly coincident) grain boundaries [20]

slight increase can be deduced for high-angle ones ($15° > \theta > 60°$). On the other hand, tin segregation is more pronounced and exhibits steep increase for low-angle grain boundaries and "saturation" of high-angle grain boundaries [526]. No systematic trend was observed in silicon segregation at twist grain boundaries [527] while a week increase of tin concentration was apparent for tin segregation at twist grain boundaries characterised by $\theta < 4°$ [526]. These studies of anisotropy of grain boundary segregation are pioneering and very instructive. Nevertheless, the studied systems were not fully characterised [526, 527]. First, not all DOFs of individual grain boundaries were fully characterised, which does not enable to construct an unambiguous structural dependence of grain boundary segregation. Second, the samples were slowly (furnace) cooled after annealing at high temperatures (1,523 K for an Fe–Si alloy and 1,670 K for an Fe–Sn alloy): It may induce an apparent solute segregation at lower temperatures so that the segregation cannot be considered as equilibrium. Third, there were other trace elements (carbon, phosphorus, sulphur) present in particular binary alloys that are able to segregate at the interfaces. These elements then affect the amount of silicon and tin at the grain boundaries and, in addition, the fracture of the samples necessary to open the grain boundaries for the AES analysis. Additionally, the fracturing was performed on air which certainly caused an intensive contamination of the fracture surfaces by oxygen and carbon. Supposing that lower segregation occurs at special grain boundaries, which may be – for simplicity – characterised by low values of Σ as compared to general ones [527], the experimental data [526, 527] allow such a construction (dashed line in Fig. 5.8) [20]. However, no significant dependence of oxygen, nitrogen and carbon segregation was observed in molybdenum [528].

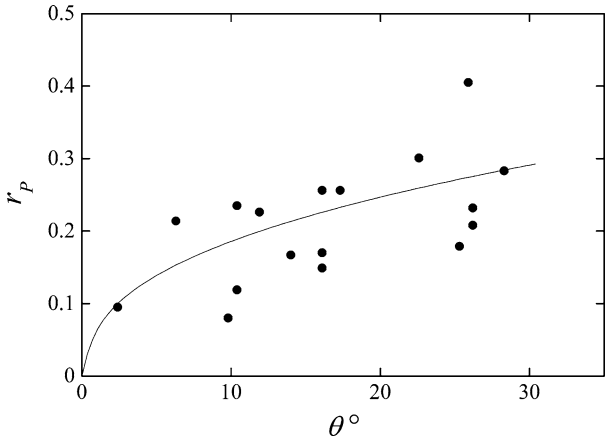

Fig. 5.9 Relation between Auger peak-to-peak height of phosphorus r_P measured on the grain boundary fracture surface of iron, and the tilt misorientation angle θ [343]

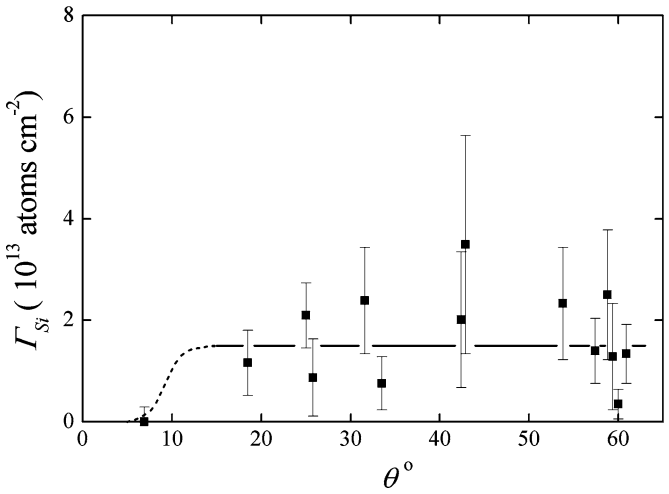

Fig. 5.10 Dependence of grain boundary concentration of silicon Γ_{Si} on the twist misorientation angle in bcc iron [241]

Phosphorus segregation in iron was found to increase with increasing tilt misorientation angle [343] (Fig. 5.9). Additionally, the level of silicon segregation at high-angle grain boundaries of bcc iron was interpreted to be completely independent of misorientation angle [241] (Fig. 5.10). These results qualitatively fit with the above-mentioned findings on silicon and tin segregation in bcc iron [526, 527] (Fig. 5.8). In case of silicon segregation in bcc iron [241] (Fig. 5.10), the summary dependence of grain boundary composition was plotted regardless the rotation axis and the grain boundary characteristics. In addition, the tendency of silicon

to segregate at grain boundaries of bcc iron is low, so, no large variations of its concentration can be expected at different grain boundaries [20]. Small amount of phosphorus was observed at low-angle and twin grain boundaries of fcc Fe–Ni–Cr alloy in comparison with general grain boundaries [529]. In case of general grain boundaries, phosphorus was found to segregate less to those oriented closely to low-index planes of one of the grains. Such boundaries were also found straight and non-facetted [529]. Similar results were also reported for phosphorus segregation in bcc iron [530].

The above-mentioned examples of orientation dependence of grain boundary segregation only qualitatively show an increase of grain boundary concentration of a solute with increasing misorientation angle of two adjacent grains. However, they say nothing instructive about the character of the anisotropy of grain boundary segregation. Increasing oxygen segregation with increasing misorientation angle of low-angle grain boundaries and its saturation was also reported for high-angle grain boundaries in molybdenum [100] tilt bicrystals [528] (Fig. 5.11a). Similarly to tin segregation in iron (Fig. 5.8), oxygen segregation was interpreted as independent of the structure of grain boundaries (full line in Fig. 5.11a). However, very few measured data only do not exclude existence of anisotropy of oxygen segregation with minima at special grain boundaries (dotted line in Fig. 5.11a) [20]. In case of [110] grain boundaries, however, cusps were already measured corresponding to the 50.5°[110], {113} and 70.5°[110], {112} grain boundaries (Fig. 5.11b).

Two maxima of bismuth segregation were found at [100] symmetrical tilt grain boundaries in copper, one at about 30°[100], the other at about 60°[100] [531]. It can also be interpreted as the dependence with a single broad minimum at about 45°[100] (Fig. 5.12). However, a detail analysis of this quite large amount of experimental data provided two sharp minima at about 37°[100] and 50°[100] misorientation angles (dotted line in Fig. 5.12) [20]. This fit could also be correlated to the orientation dependence of grain boundary energy of copper [36]. In contrast to these results, interfacial segregation of antimony in copper exhibits minima at 28.1°[100], {015}, 36.9°[100], {013}, 53.1°[100], {012} and 61.9°[100], {023} symmetrical tilt grain boundaries. These grain boundaries are also more resistant to the brittle fracture compared to the other interfaces [532].

A surprisingly reversed course of orientation dependence of the grain boundary concentration was observed in case of silicon segregation at [100] symmetrical tilt grain boundaries in 17Cr–13Ni austenitic stainless steel [533]. As shown in Fig. 5.13, the highest levels of silicon segregation were found at 36.9°[100] (Σ=5), 53.1°[100] ($\Sigma = 5$) and 67.4°[100] ($\Sigma = 13$) grain boundaries although – with respect to the atomic structure of these low-periodicity interfaces – an opposite result should be expected. Although this result seems to be strange, it may represent an exemplar consequence of the *compensation effect* (see Sect. 5.5.3).

Another important effect on the segregation properties is the orientation of the grain boundary plane. Symmetrical {111} and {112} facets of the twin grain boundary ($\Sigma = 3$) in nickel were found to be free of any segregation, while sulphur segregation was unambiguously detected at asymmetrical facets of this boundary [534, 535]. Similarly, the symmetrical {113} grain boundary does not exhibit

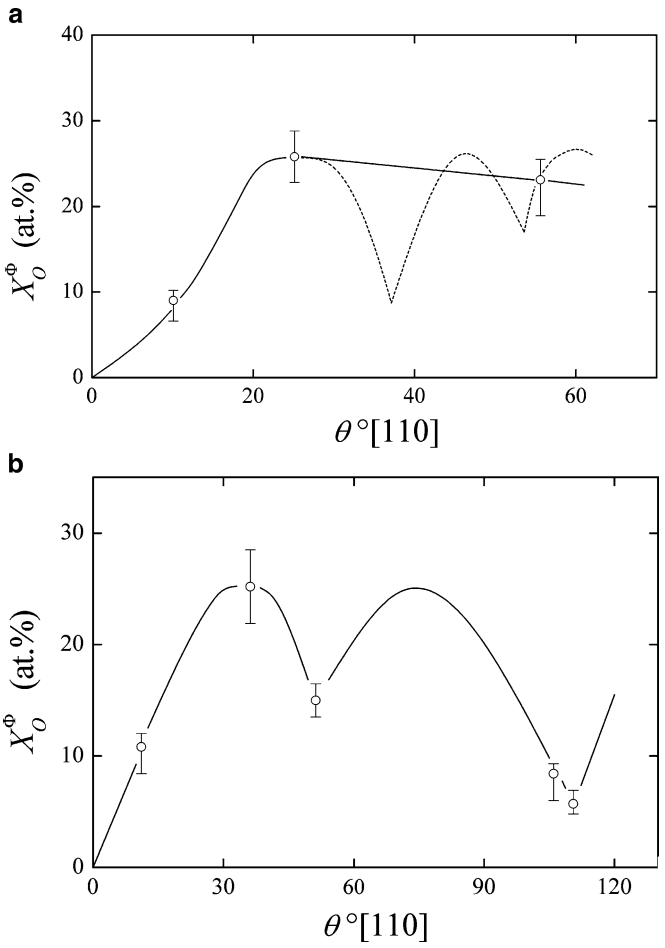

Fig. 5.11 Orientation dependence of oxygen grain boundary segregation. (**a**) [100] grain boundaries; (**b**) [110] grain boundaries [528]. The *dotted line* in (**a**) represents an alternative possible course of the dependence [20]

segregation, while the asymmetrical grain boundaries oriented closely (up to 2°) to (112)/(117), (112)/(115), (225)/(114), (113)/(114) and (116)/(112) were found enriched by sulphur [536]. In contrast to the {113} grain boundary, the other $\Sigma = 11$, {233} symmetrical tilt grain boundary in nickel was found to be very unstable and no bicrystal with this boundary could be produced. During the growth of the bicrystal with this boundary, the boundary curving occurred with the asymmetrical parts highly segregated by sulphur [537, 538]. In $YBa_2Cu_3O_{7-\delta}$, oxygen depletion is observed at the (230)/(209) grain boundary while no change of chemical composition exists at the (010)/(001) grain boundary [520].

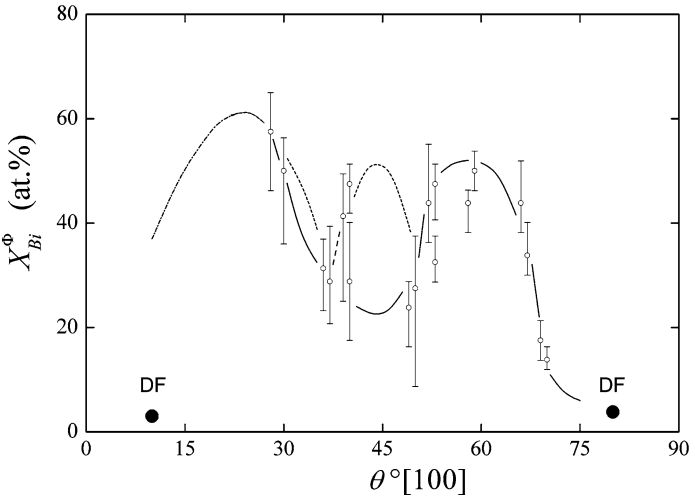

Fig. 5.12 Orientation dependence of grain boundary concentration of bismuth at [100] symmetrical tilt grain boundaries in copper at 773 K. The points DF represent ductile fracture indicating no segregation [531]. The *dotted line* suggests another interpretation of the data [20]

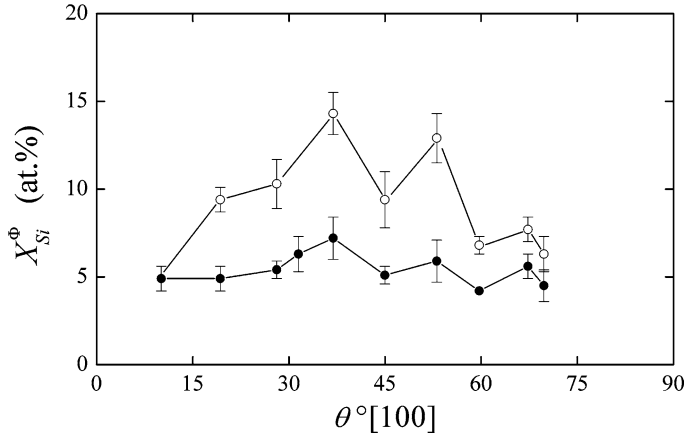

Fig. 5.13 Orientation dependence of grain boundary concentration of silicon at [100] symmetrical tilt grain boundaries in 17Cr–13Ni austenitic stainless steel containing 0.3 mass.%Si (*solid circles*) and 0.8 mass.%Si (*empty circles*) at 923 K [533]

Suzuki et al. [539] studied phosphorus segregation at grain boundaries of known orientation in polycrystalline bcc iron. In this case, phosphorus enrichment was found to be predominantly dependent on crystallographic orientation of the boundary *plane* albeit not on *misorientation angle* (Fig. 5.14). As it is indicated in Fig. 5.14, the degree of segregation was found to be large on a high-index boundary plane and low on a low-index plane, independently of the orientation of the other

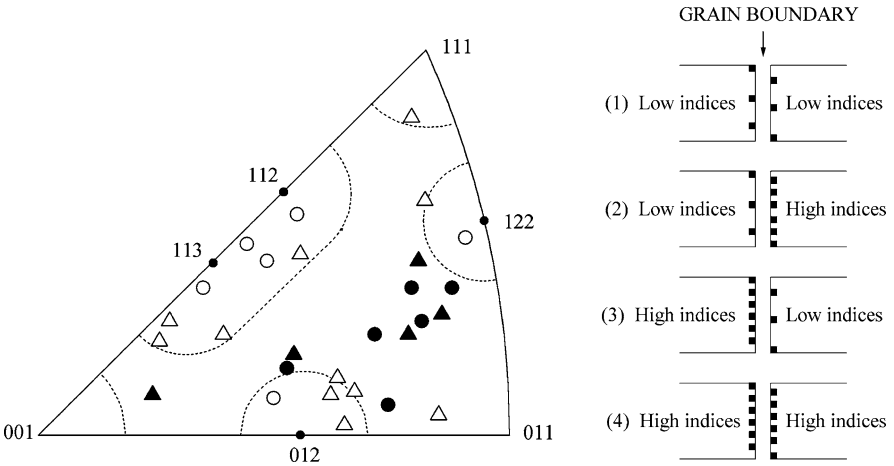

Fig. 5.14 Phosphorus segregation on grain boundaries of bcc iron [539]. (**a**) Relation between Auger peak-to-peak ratios r_P and the crystallographic orientation of grain boundary planes (*empty circles*: $r_P < 0.4$, *empty triangles*: $0.4 < r_P < 0.5$, *solid circles*: $0.5 < r_P < 0.6$, *solid triangles*: $r_P > 0.6$); (**b**) combinations of grain boundary planes with low and high index (*dark marks* schematically depict amount of segregated phosphorus)

matching boundary plane. In fact, this model is in agreement with the hypothesis of occurrence of solute segregation in different grain boundary positions [540].

Pang and Wynblatt [541] found that the strongest segregation of niobium in tetragonal rutile (TiO_2) occurs at the grain boundary planes laying along the (001)–(011)–(010) edge of the stereographic triangle, while the weakest segregation is observed for grain boundary planes close to the (110)–(010) edge.

The best way how to represent the anisotropy of grain boundary segregation precisely and independently, is an establishment of orientation dependence of its thermodynamic parameters – standard enthalpy and entropy of grain boundary segregation. Orientation dependence of the standard enthalpy of segregation of silicon, phosphorus and carbon in bcc iron can serve for an example [542]. As is seen in Fig. 5.15, this dependence for [100] symmetrical tilt grain boundaries is qualitatively similar for all three elements and is characterised by pronounced minima of $-\Delta H_I^0$ at the 22.6°[100], {015}, 36.9°[100], {013} and 53.1°[100], {012} grain boundaries. This result is in good agreement with classification of grain boundaries by means of the CSL model, because the above-mentioned grain boundaries are all characterised by low values of Σ (13, 5 and 5, respectively). However, the CSL characterisation fails when the asymmetrical grain boundaries are considered, as was already mentioned in Chap. 2. For example, the $\Sigma = 5$, 36.9°[100] tilt orientation relationship covers all types of the grain boundaries – special, vicinal and general – according to their inclination from the {013} symmetrical orientation (Fig. 5.16) [86]. The lowest tendency to segregation represented by the lowest absolute value of ΔH_I^0, was found – besides both symmetrical {013} and {012} grain boundaries – also for the asymmetrical (011)/(017) grain boundary. All these interfaces

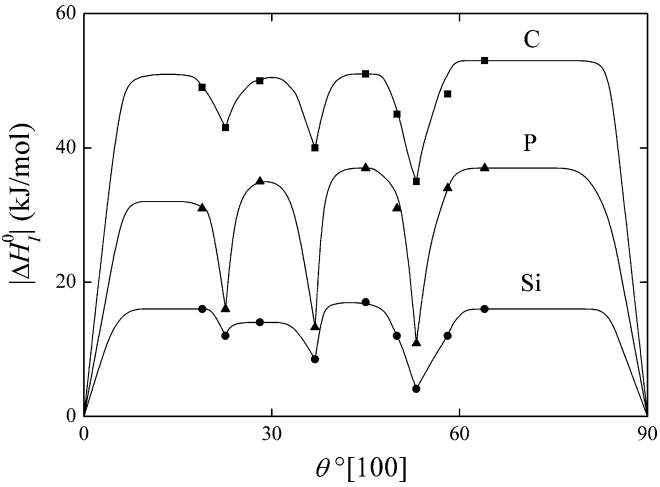

Fig. 5.15 Dependence of absolute value of the standard enthalpy of segregation of silicon (*circles*), phosphorus (*triangles*) and carbon (*squares*) on misorientation angle of [100] symmetrical tilt grain boundaries in bcc iron [542]

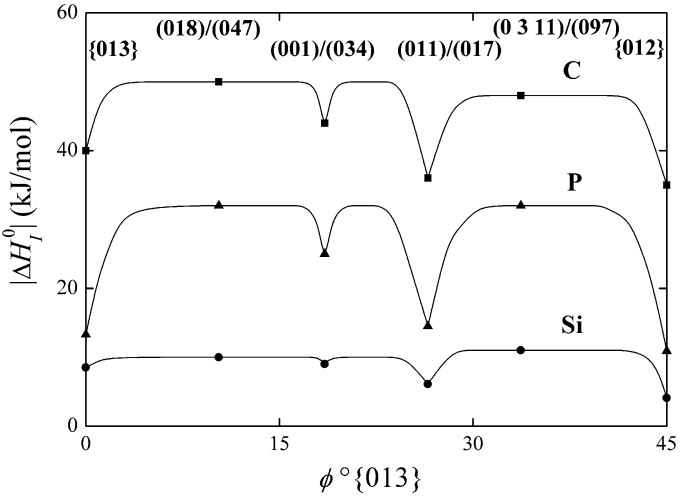

Fig. 5.16 Dependence of the absolute value of the standard enthalpy of segregation of silicon (*circles*), phosphorus (*triangles*) and carbon (*squares*) of 36.9°[100] tilt grain boundaries on inclination angle ϕ from symmetrical orientation {013} in bcc iron [86]

are considered as special. The (001)/(034) grain boundary exhibits vicinal-like behaviour, and the (018)/(047) and (0 3 11)/(097) grain boundaries are general (Fig. 5.16) [86, 94].

The differences in segregation behaviour were also found in case of two tilt grain boundaries characterised by the same non-coincidence ($\Sigma \rightarrow \infty$) 45°[100]

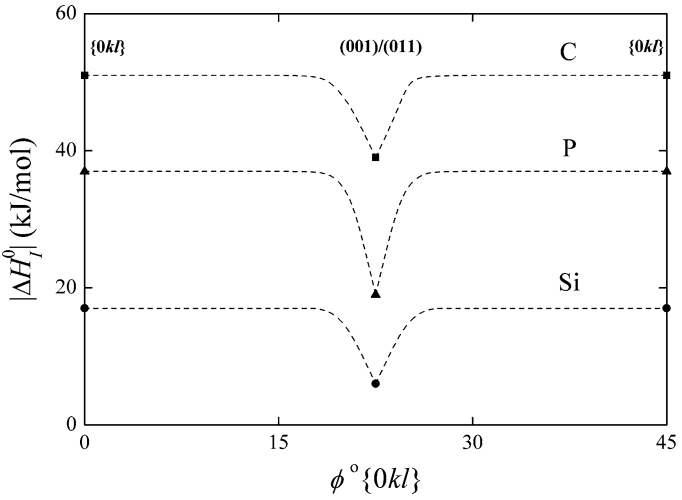

Fig. 5.17 Dependence of the absolute value of the standard enthalpy of segregation of silicon (*circles*), phosphorus (*triangles*) and carbon (*squares*) of 45°[100] tilt grain boundaries on deviation angle ϕ from symmetrical orientation $\{0kl\}$ in bcc iron [94]

orientation relationship – symmetrical $\{0kl\}$[1] and asymmetrical (001)/(011) ones. While $\{0kl\}$ behaves as typical general grain boundary, the asymmetrical grain boundary exhibits very low absolute values of the segregation enthalpy comparable with those of the {013} and {012} grain boundaries (Fig. 5.17) and, therefore, can be classified as special [87, 94, 506].

An interesting anisotropy of grain boundary segregation was also observed for asymmetrical tilt grain boundaries formed by the (001) grain boundary plane (Fig. 5.18) and the (011) grain boundary plane (Fig. 5.19). In the former case, a low tendency to segregation was indicated for the (001)/(011) and the (001)/(013) grain boundaries, while the other interfaces of this kind exhibit "transitive" values of segregation enthalpy between the level of general grain boundaries and special grain boundaries. From this point of view, they might be considered as "vicinal" [94, 98, 100]. In case of the latter interfaces, all high-angle grain boundaries possess low-absolute values of segregation enthalpy and are special [94, 98, 100]. Obtained results are in agreement with the statement of Pang and Wynblatt [541] that a boundary can exhibit strong segregation only if its matching halves also exhibit strong segregation. The results obtained for impurity segregation in bcc iron were summarised in classification of individual grain boundaries as shown in Fig. 2.9.

[1] The 45°[100] grain boundary is incommensurate and the rate k/l is irrational. Therefore, no integer Miller symbols can be found for the symmetrical interface.

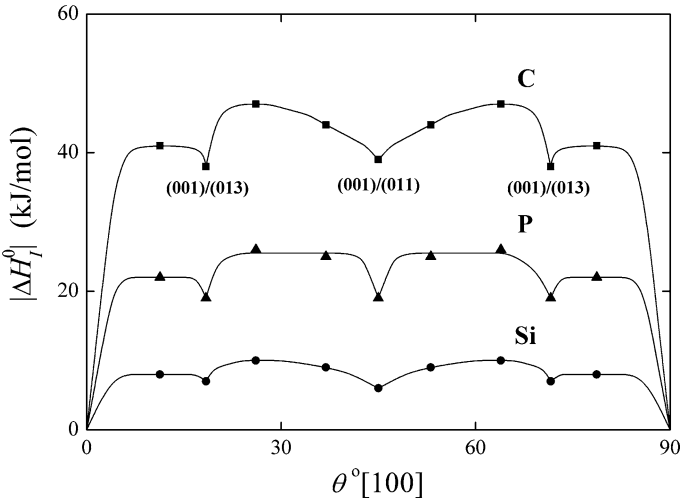

Fig. 5.18 Dependence of absolute value of the standard enthalpy of segregation of silicon (*circles*), phosphorus (*triangles*) and carbon (*squares*) of (001) asymmetrical tilt grain boundaries on misorientation angle θ of both adjoining grains in bcc iron [94]

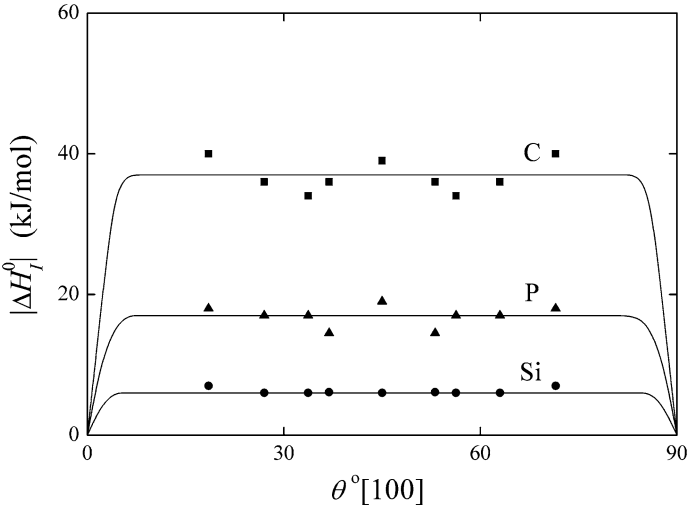

Fig. 5.19 Dependence of absolute value of the standard enthalpy of segregation of silicon (*circles*), phosphorus (*triangles*) and carbon (*squares*) of (011) asymmetrical tilt grain boundaries on misorientation angle θ of both adjoining grains in bcc iron [94]

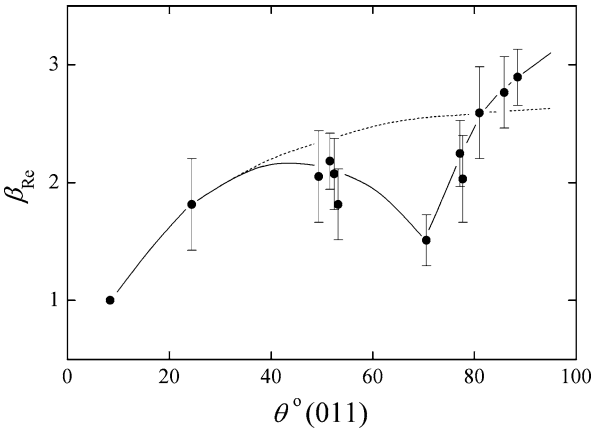

Fig. 5.20 Dependence of the enrichment factor β_{Re} for (011) twist grain boundaries on misorientation angle θ of both adjoining grains in a W–25at.%Re alloy [309]

The studies of anisotropy of solute segregation at high-angle *twist* grain boundaries are rather limited but the differences in segregation behaviour were detected as well. A minimum of rhenium segregation in tungsten at the 70.5°(011) twin grain boundary ($\Sigma = 3$) was only found in the whole misorientation range [309, 543] (Fig. 5.20) albeit not for the interface corresponding to the $\Sigma = 11$ relationship, where minims of segregation were detected for some tilt grain boundaries [309,544]. This disproportion can arise from probably larger ability of twist interfaces to grain boundary segregation as compared to tilt ones [543].

Anisotropy of solute segregation was also detected in computer simulations of the grain boundary structure and energy in binary systems. One of the first calculations of the grain boundary segregation was performed at 53.1°[100]{012} and 61.9°[100]{035} symmetrical tilt grain boundaries in Cu–Bi, Cu–Ag and Au–Ag dilute binary systems using molecular statics method [545]. The variations of the segregation energy E_{seg} (which is nearly equal to the ΔH_I) exist for different boundary sites (Table 5.1). Although both, positive and negative values of E_{seg} were found, solute segregation can only occur at those positions characterised by negative values of E_{seg} that are associated with hydrostatic tension. This suggests that bismuth segregation in copper is governed by the size effect (the atomic volume of bismuth is three times larger than that of copper). These results comply with the early model predictions of McLean [19].

The sequence of segregation of solute atoms at individual sites at a grain boundary can be documented, for example of bismuth segregation at 36.9°[100]{013} symmetrical tilt grain boundary in copper [546]. Individual grain boundary sites are shown in Fig. 5.21 and the values of E_{seg} are listed in Table 5.1. The first bismuth atom segregates at the site of type "2" (Fig. 5.21) due to the highest negative value of E_{seg}. After filling all these positions at the whole boundary, bismuth segregation proceeds at the site of type "5". After all sites "2" and "5" are occupied by bismuth,

Table 5.1 Energy (in kJ/mol) of segregation of bismuth and silver in copper, and of silver in gold at individual sites of 53.1°[100]{012} and 61.9°[100]{035} symmetrical tilt grain boundaries [545] and of segregation of bismuth in copper at 36.9°[100]{013} grain boundary [546]

System	Boundary	Boundary site					
		1	2	3	4	5	6
Cu(Ag)	{035}	+61	+82	+55	+33	+56	
	{012}	+17	+27				
Cu(Bi)	{035}	−33	+208	+43	−17	+222	
	{012}	−106	+147				
	{013}	+78	−195	+34	+68	−195	−176
Au(Ag)	{035}	−41	−40	−63	−35	−43	
	{012}	−51	−65				

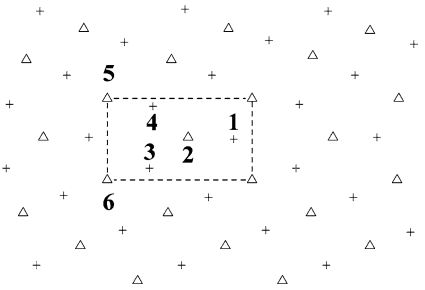

Fig. 5.21 Individual sites at the 36.9°[100]{013} grain boundary of copper [546]

a 2-D ordered structure can be distinguished in the boundary layer, where each bismuth atom is surrounded by copper atom and vice versa [546]. Similar behaviour was detected at other grain boundaries [547, 548].

A thorough theoretical study of phosphorus and boron segregation at 36.9°[100]{013} and 38.9°[110]{114} symmetrical tilt grain boundaries in bcc iron were performed by molecular dynamics calculations [281, 549, 550]. The most advantageous sites for segregation of both elements were found in the central positions of corresponding structural units – capped trigonal prism and pentagonal bipyramid, respectively. These sites are not occupied by iron atoms in the structure of pure grain boundaries and represent *interstitial* grain boundary positions. The local atomic arrangement at the respective boundaries is close to Fe_9P and Fe_7P and structurally very similar to the Fe_3P compound [551]. The values of the segregation energy [281] show high site sensitivity; however, its highest absolute value (217 kJ/mol) (Table 5.2) suggesting the most probable segregation positions for phosphorus at these grain boundaries are by about one order of magnitude higher than those of the segregation enthalpy determined experimentally not only for special {013} grain boundary (13 kJ/mol) [350] but also for general interfaces in polycrystals (21–38 kJ/mol) [328, 339, 343, 346, 552].

A rather simple method – tight-binding type electronic theory of s-, p- and d-basis orbitals – was used to study segregation of sp-valence impurities Mg, Al, Si, P and

Table 5.2 Energy (in kJ/mol) of segregation of boron and phosphorus in bcc iron at individual sites of 36.9°[100]{013} and 38.9°[110]{114} symmetrical tilt grain boundaries [281, 549, 550]

System	Boundary	Boundary site			
		1	2	3	4
Fe(P)	{013}	−208	−217	+2	−78
	{114}	−207	−190	+93	−3
Fe(B)	{013}	−236	+54	−102	−100
	{114}	−195	+20	−116	−116

Cl at the {013} grain boundary in bcc iron [270]. Calculated segregation energies for the sites at the exact boundary plane seem to depend on filling the sp-band: Maximum values of E_{seg}, suggesting the weakest segregation tendency, were found for silicon with the half-filled sp-bands. In contrast to the extremely high absolute values of the segregation enthalpy found above, the values of E_{seg} for phosphorus (−14.6 kJ/mol) and silicon (−9.8 kJ/mol) calculated in this simple way are in an excellent agreement with the values of segregation enthalpy measured experimentally for the same elements at this boundary [350] (−13.3 kJ/mol and −8.5 kJ/mol, respectively).

Similar level of the grain boundary segregation of platinum in gold represented by Γ_{Pt} was observed at corresponding $\Sigma = 5$ interfaces, 53.13°[100] {012} symmetrical tilt grain boundary and 53.13°(100) twist grain boundary at 850 K. On the other hand, five times higher segregation of platinum was surprisingly found at the above tilt grain boundary compared to the twist one in the system Ni–Pt [294].

The variations of the degree of copper segregation at various (001) twist grain boundaries of nickel using Monte Carlo simulations at 800 K showed surprisingly the strongest segregation tendency for the low-Σ misorientation in the series $\Sigma = 5$, 13 and 61 orientation relationships. The grain boundary with $\Sigma = 61$ misorientation exhibited the weakest segregation among all these boundaries [70, 553]. However, variations of chemical composition are extended in more planes parallel to the grain boundary. In case of equiatomic alloy, an oscillatory depth distribution of copper occurs, which is similar to that found for free surfaces [289, 554]. This result was confirmed using a simulation method based upon a point approximation for the configuration entropy, Einstein model for vibrational contributions to the free energy with respect to atomic co-ordinates and composition of each site [295, 555]. In addition, the segregation was found to increase with increasing (001) twist rotation angle [296].

The value of the segregation enthalpy of gold segregation at (001) twist grain boundaries of platinum were calculated as decreasing from −1.1 kJ/mol for 5°(001) grain boundary to −11.7 kJ/mol for 36.9°(001) grain boundary [70, 284]. The average enrichment ratio β_{Au} was found to depend on both temperature and misorientation angle as

$$\beta_{\text{Au}} = 1 + m(T)\sin(\theta/2) \tag{5.8}$$

with the slope $m(T)$ depending only on temperature. These Monte Carlo simulations indicate that segregation primarily occurs in cores of the grain boundary

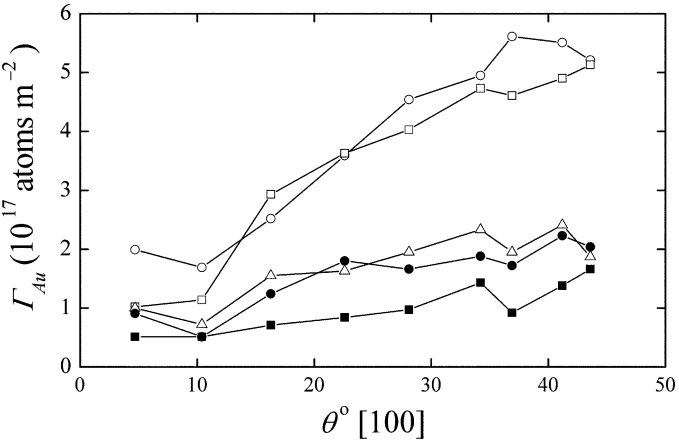

Fig. 5.22 Orientation dependence of the grain boundary concentration of gold, Γ_{Au}, at (001) twist grain boundaries on misorientation angle θ of both adjoining grains in Pt–1at.%Au alloy at 900 K (*empty circles*), 1,000 K (*empty squares*), 1,300 K (*empty triangles*), 1,500 K (*solid circles*) and 1,900 K (*solid squares*) (according to [284])

dislocations that comprise the (001) twist grain boundaries. The density of the grain boundary dislocations increases with increasing misorientation angle up to the value of about 35°: if such misorientation is exceeded, saturation establishes [284]. However, a question arises why the temperature dependence of gold segregation was theoretically found as non-monotonous in some cases (Fig. 5.22). Solute atom enrichment was also determined by Monte Carlo simulations for (001) low-angle twist grain boundaries in the Ni–Pt system. A saturation of the grain boundaries was detected at about 22°(001) grain boundary: The enrichment of the nickel boundaries by platinum is about twice higher than the nickel enrichment of platinum interfaces [285]. In contrast to this system, only gold segregation was determined by the same method at (001) low-angle twist grain boundaries in Au–Pt system on both sides of the concentration range [286].

Monte Carlo and molecular statics simulations were used to determine detail anisotropy of palladium segregation at different boundary positions of numerous special and general [110] symmetrical tilt grain boundaries in nickel [341]. The values of the segregation energy and entropy of individual sites at 23 grain boundaries were calculated. The orientation dependence of minimum average grain boundary concentration of palladium, Γ_{Pd}, is shown in Fig. 5.23. It is apparent that no segregation was calculated for the 109.47°[110] {111} symmetrical tilt grain boundary, which represents the coherent twin grain boundary. This corresponds very well with the zero-value of the energy of this grain boundary [341]. The orientation dependence of palladium grain boundary concentration copies well that of grain boundary energy except the range 50.48°–109.47°, where the increase of the grain boundary energy is not followed by appropriate increase of the palladium grain boundary concentration. Although the values of the free energy of segregation at

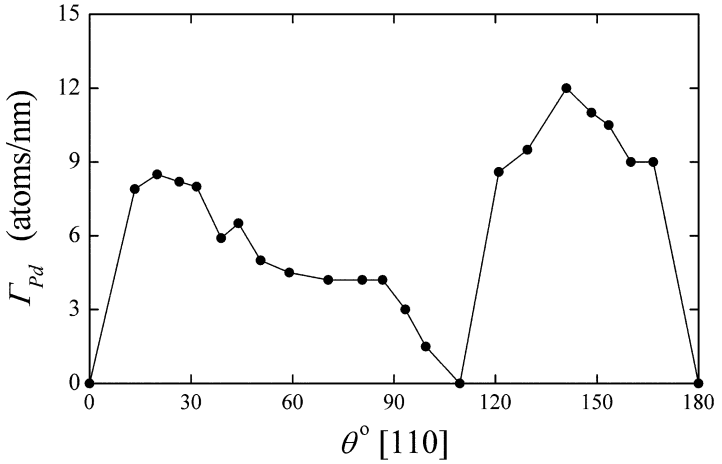

Fig. 5.23 Grain boundary concentration of palladium, Γ_{Pd}, at numerous [110] symmetrical tilt grain boundaries in Ni–4at.%Pd alloy at 800 K (according to [341])

enhanced temperature were calculated for individual grain boundary sites for the first time, no clear correlation between their values and grain boundary structure were found [341].

To elucidate the relationship between the structure and solute segregation to particular grain boundaries, high-angle grain boundaries were modelled as planar defects characterised by the thickness and the atomic density [556]. Model calculations showed that the grain boundary enrichment strongly depends on the atomic density of grain boundaries albeit not on grain boundary thickness. Therefore, a special grain boundary with the near-bulk density in simple metal will show low electronic binding energy and an important elastic binding energy. It suggests that segregation may occur at such boundaries although at low levels. Additionally, grain boundaries with small extra volume may show high adsorptive capacity. Although a change of the grain boundary density represents only one of the possible contributions to segregation, the grain boundary atomic density is considered as the most important physical parameter for segregation at periodic high-angle grain boundaries [557].

5.5 Nature of Segregating Element

5.5.1 Truncated BET Isotherm

The grain boundary energy and consequently, the Gibbs energy of segregation are also affected by the nature of the solute and the matrix element. This results in pronounced difference in segregation extent. For example, the grain boundary

enrichment ratio (4.19) of silicon in α-iron at temperatures 700–900 K was found to range between 10^1 and 10^0, while the grain boundaries of copper may accumulate 10^6 times higher amount of bismuth as compared to grain interior [307].

Seah and Hondros [307] formulated the truncated BET theory (cf. Chap. 4) for interfacial segregation in a dilute binary system as

$$\frac{X_I^\Phi}{X^0 - X_I^\Phi} = \frac{X_I}{X_I^*} \exp\left(-\frac{\Delta G_I'}{RT}\right) \tag{5.9}$$

with

$$\Delta G_I' = \Delta G_I^0 - \Delta G_I^{\text{sol}}, \tag{5.10}$$

where X_I^* is the solid solubility limit of solute I in bulk matrix M, and ΔG_I^{sol} is the Gibbs energy of solution. As it is apparent from (5.9) and (5.10) where the excess Gibbs energy term is missing, that this model assumes a non-interactive segregation in an ideal solid solution.

The truncated BET isotherm offers an interesting consequence. For low interfacial enrichment ($X_I^\Phi \ll X^{0\Phi}$), it transforms into

$$\beta_I^\Phi = \frac{X_I^\Phi}{X^{0\Phi}} \frac{1}{X_I^*} = \frac{\exp(-\Delta G'/RT)}{X_I^*}. \tag{5.11}$$

The analysis of numerous experimental data on grain boundary segregation in various binary and pseudobinary systems showed that $\Delta G'$ possesses relatively low but similar values ranging between −20 and 0 kJ/mol for all systems. Equation (5.11) can thus be simplified as

$$\beta_I^\Phi = \frac{K}{X_I^*} \tag{5.12}$$

with $K = \exp(-\Delta G'/RT)$ ranging from 1.8 to 10.8, i.e. within one order of magnitude for a wide variety of systems [13, 20, 307]. Equation (5.12) can thus be used to predict the grain boundary enrichment ratio of a solute in a matrix knowing only its bulk solid solubility (Fig. 5.24).

There are objections against the close relationship between the grain boundary segregation and the solid solubility as expressed by (5.12) and represented in Fig. 5.24. One of the most serious arguments for this disagreement results from comparison of experimental data on phosphorus and antimony segregation in bcc iron and can be summarised as follows (a) the amount of antimony segregation is much less than that of phosphorus and (b) the segregation of antimony increases with increasing bulk concentration up to the solubility limit and remains constant after reaching the solid solubility limit by bulk concentration while phosphorus enrichment of the boundary reaches its maximum for bulk concentrations below the solid solubility limit and then remains constant when the majority of primary segregation sites are occupied [336]. Another argument contra this relationship is the relatively low tendency of antimony to segregate to grain boundaries ($\Delta H_{\text{Sb}}^0 = -19$ kJ/mol) in comparison with phosphorus ($\Delta H_{\text{P}}^0 = -34$ kJ/mol) or tin ($\Delta H_{\text{Sn}}^0 = -23$ kJ/mol)

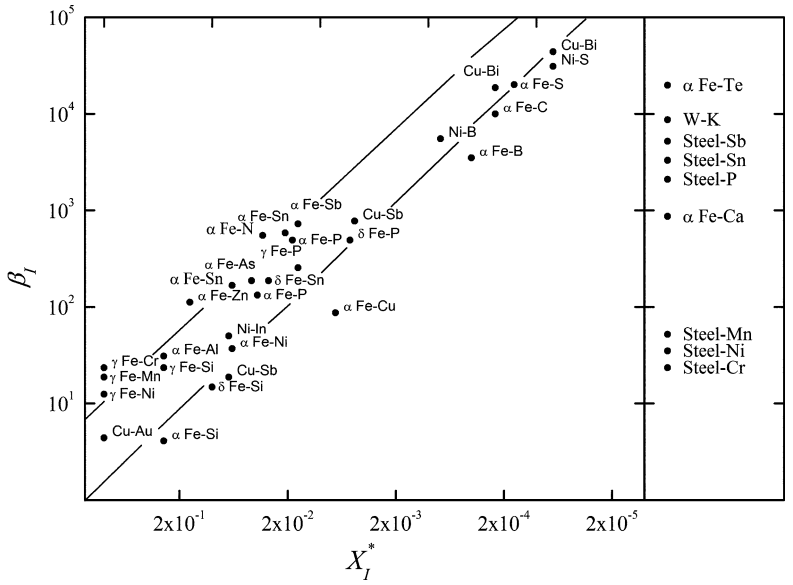

Fig. 5.24 Dependence between the experimental values of the grain boundary enrichment ratio β_I and the solid solubility X_I^* for numerous binary systems. The solid solubility of the solutes in the system given in the right column of the figure is unknown [20]

although both these elements exhibit similar solid solubility [124]. This argument is based on incorrect interpretation of the data for antimony segregation [338] as discussed in detail in Chap. 4. It is clear that (5.12) provides us with a rough estimate of the grain boundary segregation only, which does reflect neither the temperature of the grain boundary segregation nor the grain boundary structure and energy of individual sites at the grain boundary. These effects are covered by relatively large limits of the above model (within one order of magnitude as marked by solid lines in Fig. 5.24) [338]. As was shown above, the value of $\Delta H^0_{\mathrm{Sb}} = -19\,\mathrm{kJ/mol}$ showing "the low tendency to segregation" was determined under the simplified assumption $X^0 = 1$, which does not correlate the experimental data well (cf. Fig. 4.6a). When the limited saturation level is considered, a more reliable value $\Delta H^0_{\mathrm{Sb}} = -23\,\mathrm{kJ/mol}$ is obtained [338], which is identical with the segregation enthalpy of tin.

BET isotherm was also applied to correlate experimental data on sulphur and antimony segregation in iron alloys, while the correlation according to both the site competition and the Guttmann model failed [503].

5.5.2 Grain Boundary Segregation Diagram

The main drawback of the truncated BET approach is that it does not take into account the dependence of the grain boundary segregation on two main factors,

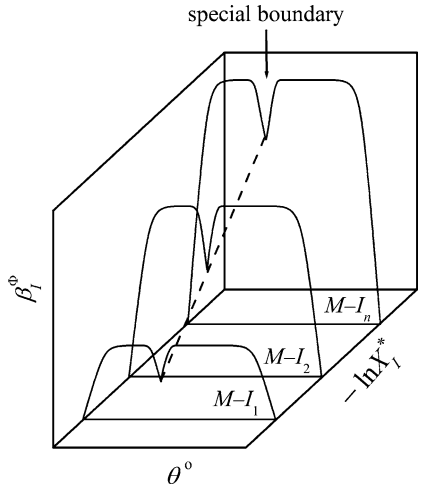

Fig. 5.25 Schematic depiction of a grain boundary segregation diagram proposed by Watanabe et al. (according to [526])

interface structure and temperature, which can alter the grain boundary concentration [20]. All these changes are supposed to be included in the scatter of K in (5.12).

Watanabe et al. [526] tried to overcome this drawback and suggested to extend the dependence between β_I^{Φ} and the solid solubility by new dimension – the grain boundary orientation. In this sense, they proposed the construction of so-called *grain boundary segregation diagrams* (Fig. 5.25).

Thermodynamic analysis of the dependence between the standard Gibbs energy of interfacial segregation, ΔG_I^0, and the solid solubility of an element in a chosen matrix, X_I^*, was done with respect to different structure of the grain boundary, Φ [17, 337, 375]. Chemical potential, μ_I^*, of the solute I in saturated bulk solid solution is

$$\mu_I^* = \mu_I^0 + RT \ln a_I^*, \tag{5.13}$$

where a_I^* is its activity in the system M–I at the solubility limit $X_I^*(T)$ [337]. We can then express the segregation free energy of the solute I, ΔG_I^*, as

$$\Delta G_I^* = \left(\mu_I^{0,\Phi} - \mu_I^*\right) - \left(\mu_M^{0,\Phi} - \mu_M^0\right) = \Delta G_I^0 - RT \ln a_I^*. \tag{5.14}$$

It can be simply shown that

$$\Delta S_I^* = \Delta S_I^0 - R\left(\frac{\partial [T \ln a_I^*]}{\partial T}\right)_{P,X_i}. \tag{5.15}$$

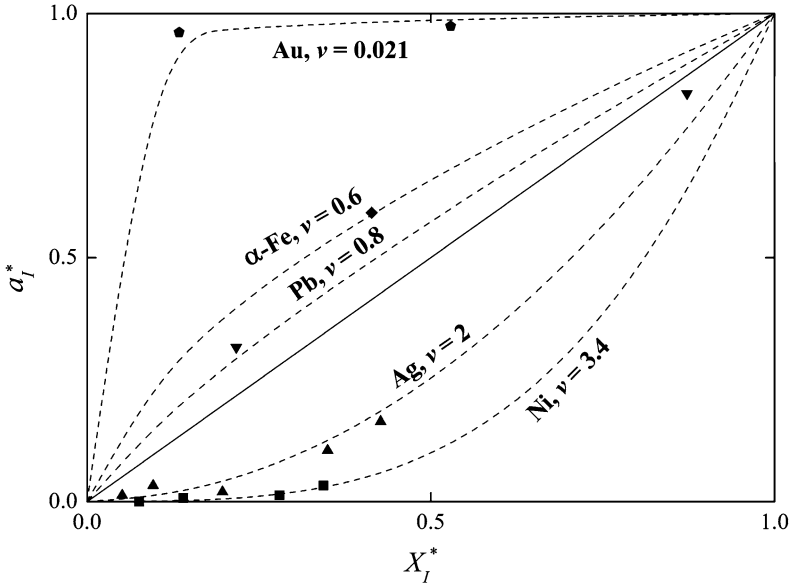

Fig. 5.26 Plot of the values of activity vs. atomic concentration of a solute at its solubility limit in α-iron [337] (data from [558])

The plot of numerous pairs of the values of activities and corresponding concentrations at the solid solubility level in various systems found in [558] revealed a simple power relationship between these two values for different systems and temperatures (Fig. 5.26),

$$a_I^* = \left(X_I^*\right)^{\nu}, \tag{5.16}$$

where the parameter ν depends on matrix element M but not on nature of the solute element I [337]. Using condition (5.15), (5.16) may be written as

$$\Delta S_I^* = \Delta S_I^0 - \nu R \left(\frac{\partial [T \ln X_I^*]}{\partial T} \right)_{P, X_i}. \tag{5.17}$$

The product on the right-hand side of (5.17), $T \ln X_I^* = \Delta G_I^{\text{sol}}/R$, was proved to be nearly independent of temperature for various systems [337, 559] (Fig. 5.27). Thus, the term in brackets in (5.17) is equal to zero and consequently, we can write (5.14) as

$$\Delta H_I^* = \Delta H_I^0 - RT \ln a_I^*. \tag{5.18}$$

As a result, the grain boundary segregation diagram can be represented by a dependence of ΔH_I^0 on both the grain boundary orientation and the product of temperature and logarithm of bulk solid solubility, i.e.

$$\Delta H_I^0(\Phi, X_I^*) = \Delta H^*(\Phi, X^* = 1) + \nu R[T \ln X_I^*(T)], \tag{5.19}$$

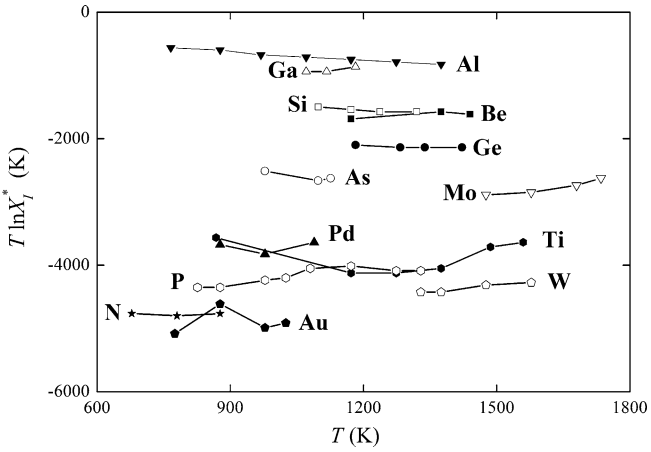

Fig. 5.27 Temperature dependence of the product of temperature and logarithm of solid solubility of various solutes in α-iron [337] (data from [560])

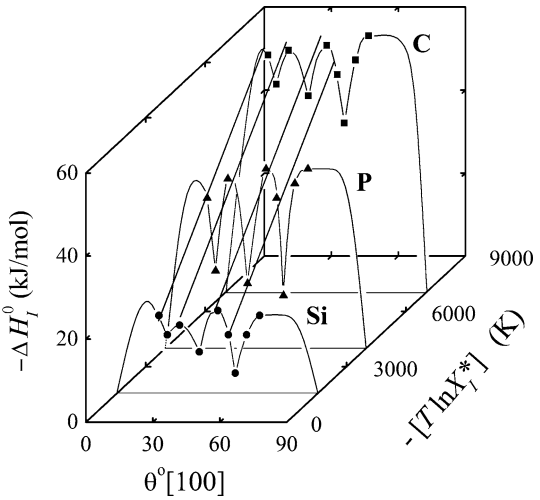

Fig. 5.28 Grain boundary segregation diagram for [100] symmetrical tilt grain boundaries in α-iron [337]

where $\Delta H^*(\Phi, X^* = 1)$ is the enthalpy of segregation of a completely soluble element at grain boundary Φ. The first experimental grain boundary segregation diagram was constructed in 1991 from the well-defined data also listed in Appendix A [337, 559].

The grain boundary segregation diagram is shown in Fig. 5.28. It is apparent that individual connecting lines (the dependence of ΔH_I^0 on the solubility term for the same grain boundary) are parallel suggesting that the two terms of the right-hand side of (5.19) are mutually independent and the slope of the dependence is the same

Table 5.3 Parameters of grain boundary segregation diagrams (5.19) for α-iron [337, 375]

Grain boundary type	ΔH^* (kJ/mol)	ν
General	−8 to −4	0.77
Vicinal	−2 to +2	0.77
Special	+5 to +8	0.77

for all grain boundaries. In fact, (5.19) represents an extension of the model of Seah and Hondros [307] by considering (a) the anisotropy of grain boundary segregation ($\Delta H_I^0(\Phi) \neq$ const.) and (b) non-ideal behaviour of the solid solutions at the solubility limit ($\nu \neq 1$) [337]. The characteristic values of ΔH^* for special, vicinal and general grain boundaries and the values of ν (5.19) in α-iron-based binary alloys [94] are listed in Table 5.3.

There are some interesting consequences of the grain boundary segregation diagrams. First, for segregation of highly soluble elements, positive values of ΔH_I^0 may appear at special grain boundaries according to the prediction. Such values have no physical meaning and therefore, it is supposed that $\Delta H_I^0 = 0$ describes such segregation most realistically [337]. Second, let us notice that the values of ΔH^* range between −8 and +8 kJ/mol for all grain boundaries (Table 5.3). This implies maximum scatter of the values of ΔH_I^0 due to segregation anisotropy to be of ±8 kJ/mol at all grain boundaries despite the character of the segregated element. It is clear because this scatter represents structural variations of the grain boundaries in the chosen matrix element.

5.5.3 Enthalpy–Entropy Compensation Effect

The *enthalpy–entropy compensation effect* is the linear dependence between the characteristic enthalpy, ΔH^{ch}, and entropy, ΔS^{ch}, of a process or equilibrium state,

$$\Delta S^{\mathrm{ch}} = a\Delta H^{\mathrm{ch}} + b, \tag{5.20}$$

where a and b are constants. Frequently, the compensation effect is also expressed as the linear dependence between the characteristic enthalpy and the logarithm of the pre-exponential factor of an Arrhenius relationship. The compensation effect is a general phenomenon detected for many processes and states in chemistry, physics, material science, biology and other fields (e.g. [12, 48, 561, 562]). Nevertheless, it is one of the concepts that cause considerable confusion and divide the scientific community to "enthusiasts" and "sceptics." The enthusiasts accept the linear enthalpy–entropy correlation and apply it in order to generalise a particular behaviour to groups of systems and propose models to explain these effects for selected phenomena mainly on basis of atomic binding (c.f. [561]). The sceptics consider it as an empirical relationship generated by statistical treatment of data [563] or as a purely mathematical consequence of the formulae employed [564]

and point out the sensitivity of the obtained data to procedure variables. Obviously, the problem in understanding arises from inappropriate application of incorrect enthalpy–entropy pairs employed in construction of the compensation graph.

The principles of the compensation effect can be elucidated by a thermodynamic analysis [48,561]. Let us assume that a "process" (chemical reaction, diffusion, ...) or an equilibrium "state" (interfacial segregation, solubility...) is controlled by a change of its characteristic Gibbs energy, ΔG^{ch}. In case of the process, ΔG^{ch} is an activation Gibbs energy, in case of the equilibrium state, ΔG^{ch} is a non-zero part of the total Gibbs energy ($\Delta G = 0$), that controls the equilibrium state. In general, ΔG^{ch} depends on N intensive variables (potentials), Ψ_j, such as electric and magnetic fields, specific defect energy, solubility and bond strength. The total differential of ΔG^{ch} in respect to the variables Ψ_j at constant temperature and pressure can be, thus, expressed as [561]

$$\mathrm{d}\Delta G^{\mathrm{ch}} = \sum_{j=1}^{N} \left(\frac{\partial \Delta G^{\mathrm{ch}}}{\partial \Psi_j} \right)_{T,P,\Psi_i \neq \Psi_j} \mathrm{d}\Psi_j . \tag{5.21}$$

Analogously,

$$\mathrm{d}\Delta H^{\mathrm{ch}} = \sum_{j=1}^{N} \left(\frac{\partial \Delta H^{\mathrm{ch}}}{\partial \Psi_j} \right)_{T,P,\Psi_i \neq \Psi_j} \mathrm{d}\Psi_j , \quad \mathrm{d}\Delta S^{\mathrm{ch}} = \sum_{j=1}^{N} \left(\frac{\partial \Delta S^{\mathrm{ch}}}{\partial \Psi_j} \right)_{T,P,\Psi_i \neq \Psi_j} \mathrm{d}\Psi_j . \tag{5.22}$$

Evidently, $\mathrm{d}\Delta H^{\mathrm{ch}}(\Psi_j)$ and $\mathrm{d}\Delta S^{\mathrm{ch}}(\Psi_j)$ are general, non-zero real numbers and therefore, a range of the changes of the variables Ψ_j must exist for that the constant temperature T_{CE} is defined as [561]

$$T_{\mathrm{CE}} = \frac{\mathrm{d}\Delta H^{\mathrm{ch}}}{\mathrm{d}\Delta S^{\mathrm{ch}}} = \frac{\sum_{j=1}^{N} \left(\frac{\partial \Delta H^{\mathrm{ch}}}{\partial \Psi_j} \right)_{T,P,\Psi_i \neq \Psi_j} \mathrm{d}\Psi_j}{\sum_{j=1}^{N} \left(\frac{\partial \Delta S^{\mathrm{ch}}}{\partial \Psi_j} \right)_{T,P,\Psi_i \neq \Psi_j} \mathrm{d}\Psi_j} . \tag{5.23}$$

It follows from (5.21) and (5.23) with (4.42) that

$$\mathrm{d}\Delta G^{\mathrm{ch}}(T_{\mathrm{CE}}) = \sum_{j=1}^{N} \left(\frac{\partial \Delta G^{\mathrm{ch}}(T_{\mathrm{CE}})}{\partial \Psi_j} \right)_{T=T_{\mathrm{CE}},P,\Psi_i \neq \Psi_j} \mathrm{d}\Psi_j = 0. \tag{5.24}$$

This provides us with a very important consequence: *at temperature* T_{CE}, ΔG^{ch} *does not change with changing variables* Ψ_i *in their specific ranges although the values of* ΔH^{ch} *and* ΔS^{ch} *may vary significantly*. Notice that at T_{CE}, ΔG^{ch} may possess any value and is not a priori equal to zero.

Integration of (5.23) results in $\Delta H^{\mathrm{ch}} = T_{\mathrm{CE}}(\Delta S^{\mathrm{ch}} + \Delta S')$ with the integration constant $\Delta S'$, and thus,

$$\Delta S^{\mathrm{ch}}(\Psi_j) = \frac{\Delta H^{\mathrm{ch}}(\Psi_j)}{T_{\mathrm{CE}}} - \frac{\Delta G^{\mathrm{ch}}(\Psi_j, T_{\mathrm{CE}})}{T_{\mathrm{CE}}}. \tag{5.25}$$

Equation (5.25), which is in its form identical with empirical (5.20), represents the mathematical form of the *compensation effect*. It suggests that the change of the characteristic enthalpy $\mathrm{d}\Delta H^{\mathrm{ch}}$ of the process caused by the change of the variable(s) Ψ_j is *compensated* by the corresponding change of the characteristic entropy $\mathrm{d}\Delta S^{\mathrm{ch}}$. T_{CE} is the compensation temperature.

As we did not specify the process or state until now, the compensation effect is general and applicable to both the dynamic processes and the equilibrium states. Therefore, it is not surprising that it is observed in many fields of science as mentioned above [561]. The presented thermodynamic treatment concerning the compensation effect is also general and does not need any assumption about its mechanism, bonding, etc. Let us stress out that the true compensation effect can exist exclusively for a well-defined single process or state and is related to unambiguously defined state conditions. In this case, the characteristic enthalpy, ΔH^{ch}, and entropy, ΔS^{ch}, must be well-defined and have clear physical meaning. In interfacial segregation, the only functions applicable for the compensation effect are ΔH_I^0 and ΔS_I^0. Here, the intensive variables Ψ_j provide constancy of the segregation mechanism. For example, the interfacial energy varies with the interface orientation but also with the nature of the segregating element. The integration constant $\Delta S' = -\Delta G_I^0(T_{\mathrm{CE}})/T_{\mathrm{CE}}$ is related to the configurational entropy of the system at T_{CE} [322, 561]. Any overlapping process such as species interactions have to be avoided because it may provide an additional complex contribution to the values of ΔH^{ch} and ΔS^{ch} and therefore, it may result in a mechanism differing from that for which the compensation effect is considered.

This can be documented in Fig. 5.29 by comparing the plots of the values of ΔS_{C}^0 vs. ΔH_{C}^0 of carbon segregation at symmetrical tilt grain boundaries of α-iron [94] with the values of the segregation enthalpy and entropy, ΔS_I vs. ΔH_I [113]. Since the values of both ΔS_I^0 and ΔH_I^0 are principally independent of temperature (and concentration), there is no indication of temperature. It is apparent that this plot exhibits a pronounced linear dependence between ΔS_{C}^0 and ΔH_{C}^0 (Fig. 5.29a) albeit not between ΔS_I and ΔH_I for carbon at 923 K (Fig. 5.29b). This is because the latter thermodynamic functions involve two contributions to the actual segregation of carbon (a) the tendency of carbon to segregate at grain boundaries of iron in infinitesimally diluted (ideal) solid solution and (b) the interaction of carbon with other segregating elements, phosphorus and silicon. Figure 5.29 clearly demonstrates the above mentioned necessary condition of the linear dependence between characteristic enthalpy and entropy – its exclusivity for a single, well-defined mechanism of the process or state [561].

The range of existence of the compensation effect (i.e. $T_{\mathrm{CE}} = \mathrm{const}$) for grain boundary segregation in α-iron, represented by correlated pairs of ΔH_I^0 and ΔS_I^0, is quite large covering very different grain boundaries and also different segregating elements (Fig. 5.30) [561]. As is clearly seen in Fig. 5.30, the linear dependence between ΔH_I^0 and ΔS_I^0 is very well fulfilled not only for individual

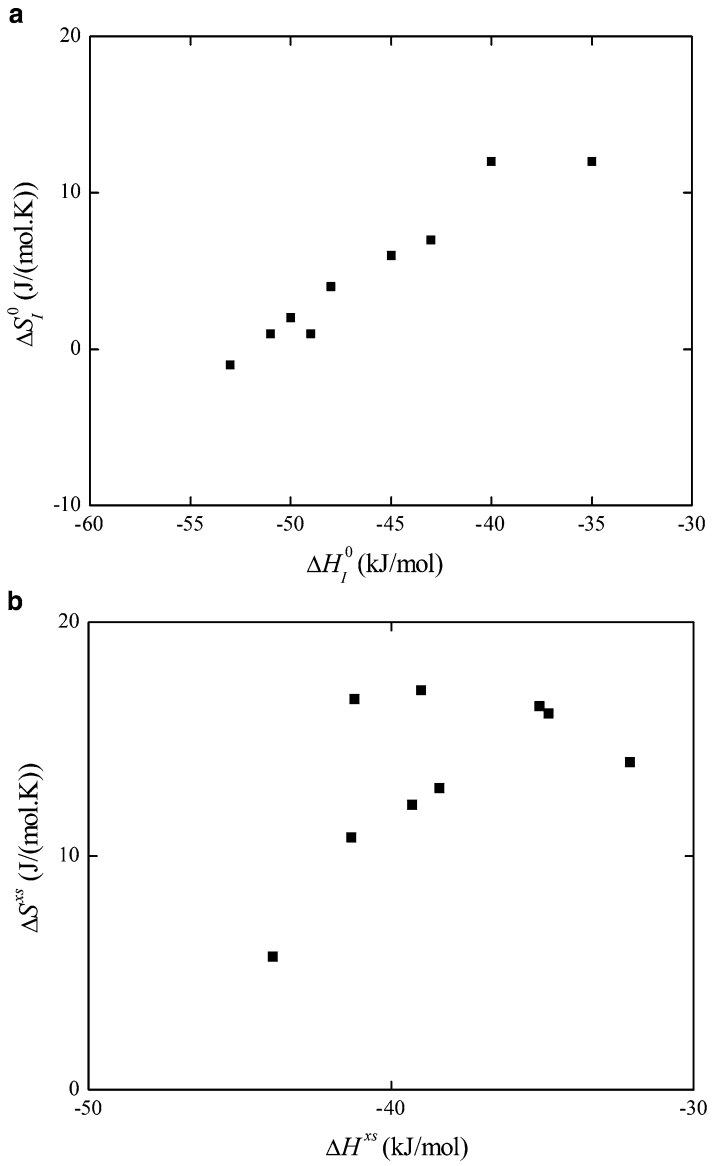

Fig. 5.29 Interdependence of characteristic entropy and enthalpy of segregation of carbon at well-characterised symmetrical tilt grain boundaries in α-iron. (**a**) Standard entropy and enthalpy of carbon segregation, ΔS_C^0 and ΔH_C^0, and (**b**) entropy and enthalpy of carbon segregation, ΔS_C and ΔH_C, at 923 K (according to [113])

grain boundaries (sites) in case of carbon, phosphorus and silicon segregation in α-iron (solid symbols) [98, 565] but also for various other solutes segregating preferentially at general interfaces in polycrystals [561]. The compensation effect for interfacial segregation splits into two branches reflecting, thus, two different atomic

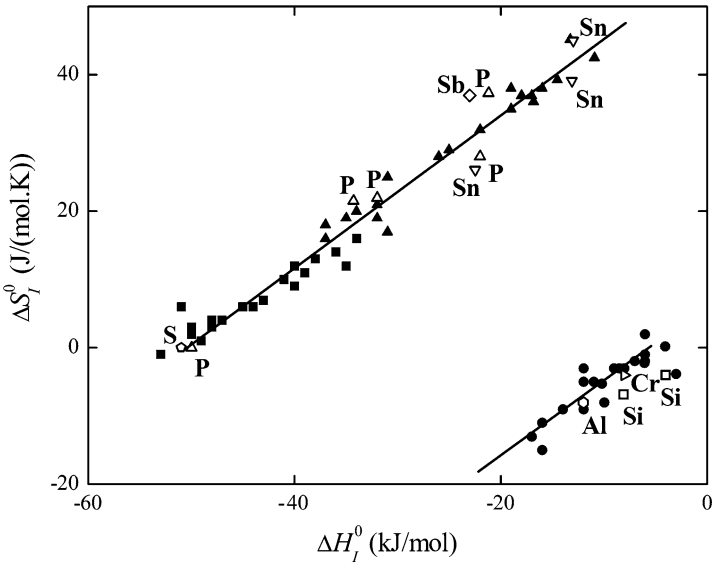

Fig. 5.30 Dependence of the standard molar entropy, ΔS_I^0, and the standard molar enthalpy, ΔH_I^0, of grain boundary segregation in α-iron. *Full symbols* depict segregation of carbon (*squares*), phosphorus (*triangles*) and silicon (*circles*) at individual grain boundaries, the *empty symbols* represent the data measured in polycrystalline iron ("average" grain boundaries) that were found in literature. The upper and lower branches of the dependence represent the best fits of the data on solute segregation at interstitial sites and in substitutional positions, respectively [97, 565]

mechanisms of grain boundary segregation – interstitial (upper branch) and substitutional (lower branch) [98]. This proves the sensitivity of the compensation effect to the character of the single process for which the compensation effect can exist. The value of $T_{CE} = 930$ K remains, however, identical for both branches of the compensation effect suggesting that the compensation temperature is a characteristic of the matrix element ($\Delta G_I^0(T_{CE})/T_{CE} = -56$ J/(mol K) and -5 J/(mol K) were deduced for interstitial segregation and for substitutional segregation, respectively). Due to wide existence of the compensation effect it can also be used to predict the values of ΔH_I^0 and ΔS_I^0 for many grain boundaries and many segregating elements (see Sect. 5.7.1) [375].

Although the nature and physical meaning of the compensation temperature is still open for discussion at present, its existence is well established and has a very interesting and important consequence. According to (5.24), $\Delta G_I^0(T_{CE}) = \text{const}$ for all interfaces (and also for different solutes segregating at the interfaces supposing identical mechanism of segregation – substitutional or interstitial). It means that there exists a joint cross-section of ΔG_I^0 on its temperature dependence for different grain boundaries as indicated in Fig. 5.31. It means that for two interfaces (sites), A and B, for which ${}^{A}\Delta G_I^0(T_1) < {}^{B}\Delta G_I^0(T_1)$ at $T_1 < T_{CE}$, the reverse relationship is valid at $T_2 > T_{CE}$, ${}^{A}\Delta G_I^0(T_2) < {}^{B}\Delta G_I^0(T_2)$. This is obvious from

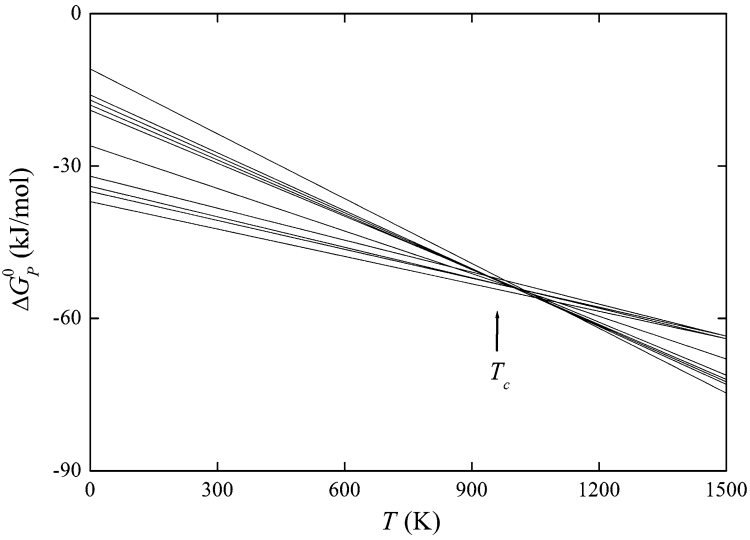

Fig. 5.31 Temperature dependence of the standard molar Gibbs energy of phosphorus segregation, $\Delta G_{\mathrm{P}}^{0}$, in α-iron at various grain boundaries (data from [94])

Fig. 5.32 for phosphorus segregation at grain boundaries in an Fe–Si–P–C alloy [94]. This is also supported by much higher silicon segregation at {013}, {012} and {023} special grain boundaries in austenitic stainless steel as compared to general ones [533] (Fig. 5.13). We may well deduce that these measurements were performed at $T > T_{\mathrm{CE}}$. Existence of the compensation effect confirms the importance of the segregation entropy in interfacial segregation that cannot be neglected in any case.

A clear enthalpy–entropy compensation effect was also detected for palladium segregation at different sites in different grain boundaries of nickel obtained from computer simulations [341]. However, the type of their enthalpy and entropy terms is not completely clear: Because it is assumed in [341] that both functions are independent of temperature, one should suppose that these data represent the effective $\Delta H_{\mathrm{seg}}^{\mathrm{eff}}$ and $\Delta S_{\mathrm{seg}}^{\mathrm{eff}}$. Only when $\Delta G_I(T)$ deviates negligibly from a linear dependence on temperature these values could be considered as equivalent to ΔH_I^0 and ΔS_I^0. However, this information is not known. The results suggest that in the above case of Ni–Pt, (a) the averaging over a temperature range does not play important role and (b) the segregation mechanism is considered identical for all grain boundaries (grain boundary sites). Therefore, the necessary conditions of the compensation effect are fulfilled. The compensation effect was also reported for gold segregation at nickel surface [567].

It should be emphasised that special care is necessary in selecting appropriate data to verify the compensation effect. All fundamentals have to be well understood before making general conclusions, particularly in constructing arguments against the importance of the compensation effect.

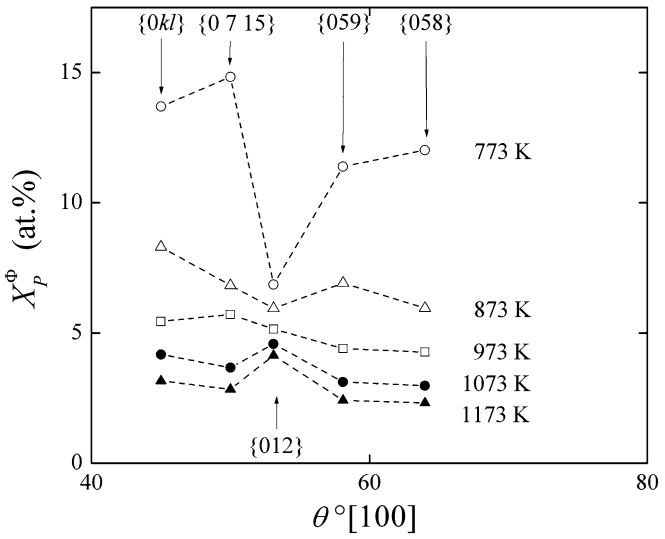

Fig. 5.32 Dependence of phosphorus concentration at [100] symmetrical tilt grain boundaries in an Fe–3.55at.%Si–0.0089at.%P–0.014at.%C alloy on misorientation angle at various temperatures [566]

5.6 Grain Size

The size of individual grains in a polycrystalline material does not belong among intensive thermodynamic parameters affecting interfacial segregation of solutes. In a wide range of the coarse grain size, it also does not affect the interfacial segregation. It is because the total number of the interfacial positions available for segregation in coarse-grained materials is negligible compared to the amount of the solute atoms in grain volume [568]. However, the grain size becomes important for the segregation effects if it reaches the nanometer range. In this case, the fraction of the grain boundary sites substantially increases and consequently, the grain boundaries become strongly curved. As shown by Siegel [569], the volume fraction of the grain boundaries is approximately 25% for the material with the grain size of 10 nm and approximately 50% for the grain size of 5 nm supposing the thickness of the grain boundary being 1 nm. Thus the amount of the grain boundary positions available for segregation is comparable with the volume sites. As a consequence, segregation of the solute atoms at the grain boundaries evokes reduction of the bulk concentration to one-half. This implies that the solute segregation is strongly suppressed in nanocrystalline materials. It also means that the solubility of a solute in nanocrystalline materials will be enhanced comparing to the classical fine-grained polycrystals [569, 570]. This was confirmed by the finite element simulations of the kinetics of sulphur segregation at grain boundaries of nickel. This simulation showed that the saturation level of more than 80 at.% of sulphur is reached in nickel with bulk concentration of sulphur of 20 ppm at 800 K if the grain size is 1 mm or

0.1 mm. However, if the grain size is lowered to 10 μm, maximum sulphur segregation reaches 30 at.% and in case of the grain size of 1 μm, the sulphur segregation reaches only less than 5 at.% [571].

The total concentration of the solute atoms in a polycrystalline material, X_I^{p}, is given as [568]

$$X_I^{\mathrm{p}} = X_I f + X_I^{\Phi}(1 - f), \tag{5.26}$$

where f is the volume fraction of the grain boundaries. In conventional materials (bicrystals, general grain boundaries in polycrystals, see Chap. 4), the number of available positions for segregation is negligible comparing to that of the amount of the solute atoms and therefore, the bulk concentration X_I does not change during the segregation process so that $X_I^{\mathrm{p}} \cong X_I$. Rigorously, the volume fraction of the grain boundaries can be expressed as [568]

$$f = \frac{\delta}{2} \times \frac{4\pi \bar{r}^2}{\frac{4}{3}\pi \bar{r}^3} = \frac{3\delta}{2\bar{r}}, \tag{5.27}$$

where δ is the grain boundary thickness and $\bar{r}$ is the average grain radius. Introducing (5.27) into the Langmuir–McLean segregation isotherm, (4.61), we obtain

$$\frac{X_I^{\Phi}}{1 - X_I^{\Phi}} = \frac{X_I^{\mathrm{p}} - \frac{3\delta}{2\bar{r}} X_I}{1 - X_I^{\mathrm{p}} - \frac{3\delta}{2\bar{r}}(1 - X_I)} \exp\left(-\frac{\Delta G_I}{RT}\right). \tag{5.28}$$

In conventional materials, $3\delta/2\bar{r} \ll 1$, (5.28) is identical to (4.38). Using this model, Ishida [568] showed that the extent of variations in the grain boundary segregation is negligible for the grains larger than 300 μm. However, the critical value will be different for particular segregation systems. On the other hand, a clear size dependence of calcium segregation was found at grain boundaries of synthesised rutile below the critical size of 150–350 nm. In case of larger grain size, the grain boundaries were found to be saturated by calcium at the level of about one-half of a monolayer [570]. Theoretical calculations suggest that there is no practical change in grain boundary segregation of sulphur in nickel polycrystals with the grain size larger than 100 μm; however, it is about three times lower when the grain size is reduced to 10 μm and about 20 times lower in case of 1 μm grain size [182, 572].

Solute diffusion of silver in nanocrystalline γ-Fe–40mass%Ni alloy revealed its strong segregation characterised by $\Delta H_{\mathrm{Ag}} = -47$ kJ/mol. This value is comparable with that found for coarse-grained polycrystals [573].

At lower temperatures and small grain sizes, there exists a critical concentration, X_I^{c},

$$X_I^{\mathrm{c}} = X_I^{\mathrm{p}} \frac{2\bar{r}}{3\delta} \tag{5.29}$$

representing the state when all solute atoms segregate at the grain boundaries. Corresponding relationships can be derived for multi-component systems [568].

Cerium, calcium and strontium effectively segregate at the grain boundaries of AZ91 magnesium-based alloy and suppress the grain growth in this material.

Alloying with pure cerium causes reduction of the grain size from 107 to 36 μm in as-cast material. After a suitable mechanical and thermal treatment, the grain size was further reduced to 20 and 30 μm using combination of cerium with calcium and with strontium, respectively [574].

Thermodynamic analysis performed by Weissmüller [575] revealed a very important feature in the field of *nanocrystalline* materials – an existence of a state where the alloy is stable with respect to the variation of the total grain boundary area. For a nanocrystalline material, the Langmuir–McLean segregation isotherm was extended to yield the total Gibbs energy of an alloy nanocrystal, G^{nx}, as function of pressure P, temperature T, concentrations of solvent M and solute I, and of the total grain boundary area A. Supposing random substitutional solid solution with crystal volume and the grain boundaries with fixed numbers of sites $N = N_I + N_M$ and $N^\Phi = N_I^\Phi + N_M^\Phi$, the Gibbs energy of the system is given as

$$G^{nx} = \left(N_I + N_I^\Phi\right)\mu_I^0 + \left(N_M + N_M^\Phi\right)\mu_M^0 + \sigma^0 A + N_I \Delta H^{\text{sol}}_{I\,\text{in}\,M} + N_I^\Phi \Delta H^{\text{sol}}_{I\,\text{in}\,\Phi} + RT\left[N_I \ln\left(\frac{N_I}{N}\right) + N_M \ln\left(\frac{N_M}{N}\right) + N_I^\Phi \ln\left(\frac{N_I^\Phi}{N^\Phi}\right) + N_M^\Phi \ln\left(\frac{N_M^\Phi}{N^\Phi}\right)\right], \tag{5.30}$$

where σ^0 is the grain boundary energy in pure solvent, both at chosen temperature and pressure. Stirling formula was applied to the logarithms of N_i-factorials.

Supposing, for simplicity, spherical grains in a polycrystal, the grain boundary area A can be related to the crystal volume V as $A \approx 3V/2\bar{r}$. The detail treatment of the problem shows that G^{nx} reduces with decreasing $\bar{r}$, because the increase of the grain boundary energy connected with the decrease of the grain size is less than the decrease of the Gibbs energy connected with the solute segregation. At very low grain sizes, however, G^{nx} increases again because the majority of the solute atoms are already present at the grain boundary and the grain boundary area further increases. Thus the boundary energy then prevails over the gain in reduction of the Gibbs energy due to segregation. As a result, there exists a minimum of G^{nx} for a grain size $\bar{r}$ in nanometer range [575].

The existence of a minimum of the Gibbs energy suggests the segregation-induced stability of nanosized materials, for example stopping the grain growth when this "equilibrium" size is reached [576]. This inhibition and, thus, stabilisation of the grain size in the nanometer range is of high importance for advantageous applicability of nanocrystalline materials. According to (4.15) the grain boundary adsorption is related to the change of the grain boundary energy with the change of the chemical potential. Supposing an ideal solid solution and Henry law for the solvent, we can rewrite (4.15) as [577]

$$\left(\frac{\partial \sigma}{\partial X_I}\right)_{T,P} = -\frac{\Gamma_{I,M}^\Phi RT}{X_I}. \tag{5.31}$$

Integration of (5.31) results in

$$\sigma - \sigma_0 = -RT\delta\rho X^{0\Phi}\left[1 + \frac{1}{\exp\left(-\Delta G_I^0/RT\right)-1}\right] \times \ln\left[1 - X_I + X_I \exp\left(-\frac{\Delta G_I^0}{RT}\right)\right], \tag{5.32}$$

where ρ is the density and δ is the thickness of the grain boundary. In (5.32) the Langmuir–McLean segregation isotherm (4.61) was also applied. Assuming for simplicity $\left|\Delta G_I^0\right| \gg RT$, (5.32) may be written as

$$\sigma = \sigma_0 - \Gamma^{0\Phi}\left[RT \ln X_I - \Delta G_I^0\right]. \tag{5.33}$$

In (5.33) $\Gamma^{0\Phi} = X^{0\Phi}\delta\rho$ is the Gibbs adsorption in saturation. The main message of (5.32) is that σ decreases from the value of σ_0, because the Gibbs energy of grain boundary segregation, ΔG_I^0, is essentially negative. In a real system, a segregation isotherm should be used accounting for interaction in the system, e.g. the Fowler isotherm ((4.32) and (4.79) for a binary system).

To relate X_I to the grain boundary area A or to the grain size, we can again suppose for simplicity the spherical grains with an average radius $\bar{r}$. Then

$$X_I = X_I^{\mathrm{p}} - \frac{3V\Gamma_{I,M}^{\Phi}}{2\bar{r}} \tag{5.34}$$

with V being the molar volume of the alloy [577]. According to (5.34), the changes in grain size represented by $\bar{r}$ evoke changes in volume concentration of solute I as already proposed above. According to (5.33) and (5.34), the grain size $2\bar{r}^*$ corresponding to the metastable state is

$$\bar{r}^* = \frac{3V\Gamma_{I,M}^{\Phi}}{2\left[X_I - \exp\left(\frac{\sigma_0 + \Gamma^{0\Phi}\Delta G_I}{RT\Gamma^{0\Phi}}\right)\right]}. \tag{5.35}$$

Under the conditions of (5.35), the grain boundary energy is equal to zero [577]. Such a boundary is then intact and thus rather stable. Indeed, any change of external conditions (temperature, pressure, magnetic field...) causes a disturbance of this state and further process leading either to reaching another metastable state or the equilibrium one [578]. Knowledge on the relationship between the level of grain boundary segregation, grain size and thermal condition may be successfully used to predict the metastable grain size of a nanocrystal [567, 579, 580].

Stabilization of nanocrystalline grain sizes up to the temperatures close to the melting points was reported for Pd–Zr [581], Fe–Zr [582] and Cu–Nb [583] alloys. In case of the grain size stabilization in Pd–Zr and Fe–Zr alloys, the thermodynamic reasons for the stabilization seem to be important [584]. The behaviour of the Cu–10 at.% Nb alloy is more complex because of presence of niobium second phase particles in metastable solid solution of niobium in copper. Nevertheless, the 50 nm size of the grains did not change even after annealing at 1,000 °C, i.e. at

$0.94T_{\mathrm{m}}$ [583] proving that nanocrystalline grain structures can be stabilised up to the temperatures near the melting point [584].

Shvindlerman and Gottstein considered the relationship between the grain size and the grain boundary volume [585]. The Gibbs–Duhem expressions for an interface can be written at constant temperature as

$$\mathrm{d}\sigma = -\sum_{i}^{k} \Gamma_i^{\Phi} \mathrm{d}\mu_i, \tag{5.36}$$

i.e.

$$\mathrm{d}\sigma = -\Gamma_0^{\Phi} \Omega \mathrm{d}P, \tag{5.37}$$

where Γ_0^{F} is the auto-adsorption in one-component system and Ω is the atomic volume. Evidentially,

$$\frac{\mathrm{d}\sigma}{\mathrm{d}P} = -\Gamma_0^{\Phi} \Omega. \tag{5.38}$$

The grain boundary volume, ΔV^{Φ}, can be written as

$$\Delta V^{\Phi} = \frac{3}{2\bar{r}} \Gamma_0^{\Phi} \Omega. \tag{5.39}$$

The force $F_{\Delta V^{\Phi}}$ on the grain boundary is

$$F_{\Delta V^{\Phi}} = \frac{3}{2\bar{r}} P \Gamma_0^{\Phi} \Omega. \tag{5.40}$$

Analogously to (5.26) the Gibbs energy of the polycrystal is

$$\Delta G = (V_0 - A_{\mathrm{t}}\delta)\Delta G_{\mathrm{sol}}(X_I) + \sigma(X_I) A_{\mathrm{t}}, \tag{5.41}$$

where $\Delta G_{\mathrm{sol}}(X_I)$ is the formation Gibbs energy of the system with the concentration X_I, V_0 is the sample volume, A_{t} is the total grain boundary area and δ is the grain boundary thickness. Actual impurity concentration of I in the grain is

$$X_I = \frac{V_0 X_I^{\mathrm{p}} - X_I^{\Phi} A_{\mathrm{t}} \delta}{V_0 - A_{\mathrm{t}}\delta}, \tag{5.42}$$

where X_I^P is the concentration of I in the sample. When A_{t} increases due to reduction of $\bar{r}$, V_0 becomes comparable to the product $A_{\mathrm{t}}\delta$ and the term of $\Delta G_{\mathrm{sol}}(X_I)$ approaches to zero [585]. Then

$$\frac{\mathrm{d}\Delta G}{\mathrm{d}A_t} \approx \sigma(X_I). \tag{5.43}$$

If the grain boundary segregation could substantially reduce the grain boundary energy so that $\sigma(X_I) \approx 0$, ΔG reaches minimum in respect to A_t and corresponding grain size is equilibrium. This case could be considered as *grain size stabilization by segregation*. However, this situation has not been observed till now and the driving force for grain growth always exists.

Recently, an analytical model was proposed by Trelewicz and Schuh [586] which is based on statistical mechanical approach to a regular solution model for a binary polycrystalline system supposing grain size is a state variable. According to this model, the energetics of the system is strongly affected by solute segregation in such an extent that it should control the equilibrium grain size. Enhanced bulk concentration of the solute results in increased segregation, which should further reduce the grain size of the polycrystal [586].

In connection with the nanocrystalline materials, one has to think about the structure of grain boundaries connecting small grains. Such interfaces are in no means planar and will cover wide ranges of orientations [569]. Many experimental studies disclosed that atomic structures of these grain boundaries may be considered as random and do not possess any order normally found in grain boundaries of conventional coarse-grained polycrystals [569, 584].

5.7 Prediction of Grain Boundary Segregation

Knowledge on grain boundary segregation in a variety of systems including multicomponent alloys is important for many applications, for example to disclose detrimental effects of rarely used alloying elements on brittleness, corrosion resistance or electric conductance in technological materials. Therefore, appropriate measurements of grain boundary segregation are necessary to elucidate these aspects. In cases when the measurement of grain boundary concentration may become impossible from technical reasons (cf. Chap. 3), any estimate of the grain boundary segregation is welcome.

5.7.1 Model of Lejček and Hofmann

Obviously, the values of the enthalpy and entropy for each involved solute and for each grain boundary (or boundary site) are necessary to completely describe the grain boundary segregation. In the diluted (ideal) limit, the values of ΔH_I^0 and ΔS_I^0 are satisfactory. Their values for segregation of any solute at any grain boundary can be predicted on basis of the above-mentioned grain boundary segregation diagrams $\left(\Delta H_I^0\right)$ and using the compensation effect $\left(\Delta S_I^0\right)$.

The prediction procedure is very simple: From a phase diagram (e.g. [560]), the solubility of a solute in the matrix element can be read at any temperature. Knowing the values of v and ΔH^* (for α-iron these values are given in Table 5.3), the values of

ΔH_I^0 can be completely determined according to (5.19). Knowing the value of T_{CE} and of $\Delta G_I^0(T_{CE})/T_{CE}$ depending on the type of solute segregation (interstitial or substitutional), the values of ΔS_I^0 can be obtained using (5.25) (for above-mentioned case of α-iron, $T_{CE} = 930\,\text{K}$ and $\Delta G_I^0(T_{CE})/T_{CE} = -56\,\text{J/(mol K)}$ for interstitial segregation and $\Delta G_I^0(T_{CE})/T_{CE} = -5\,\text{J/(mol K)}$ for substitutional segregation, cf. Sect. 5.5.3). According to (4.42) and (4.66) we can then estimate the values of the concentration of this solute at chosen grain boundaries for any temperature and bulk concentration (within the range of existence of the solid solution) [375].

The values of ΔH_I^0 and ΔS_I^0 for segregation of numerous solutes at chosen grain boundaries in α-iron are listed in Appendix B.

For more concentrated (real) solid solutions, a correction to mutual interaction has to be made resulting in the values of ΔH_I and ΔS_I.

The predicted interfacial segregation can be compared with the experimental data using the values of ΔG_I^0, ΔH_I^0 and ΔS_I^0, or with X_I^Φ of some solutes in α-iron-based binary systems published in literature. Usually, such data were most often obtained by AES measurements on polycrystalline samples. Because the segregation enthalpy and entropy data listed in some publications are not well specified and obviously possess non-standard character, it is necessary to correct for interactions or site limitations in order to obtain values that really represent the standard Gibbs energy or enthalpy and entropy of segregation required for a meaningful comparison. The predicted values are not compared to computer simulations as these results frequently represent the values for ΔG_I, ΔH_I and ΔS_I.

As regards the solutes segregated in substitutional sites, Table 5.4 shows an excellent agreement between prediction and experiment for *aluminium* and *silicon*, and fairly good agreement for *chromium* and *molybdenum*. The differences between the predicted and the experimental values of ΔH_{Cr}^0 and ΔS_{Cr}^0 are within the experimental error ($\pm 5\,\text{kJ/mol}$ and $\pm 5\,\text{J/(mol K)}$), the predicted and experimental values of ΔG_{Cr}^0 differ only by 1 kJ/mol. The value $\Delta G_{Mo}^0 = -20\,\text{kJ/mol}$ differs substantially from the prediction; however, this value was determined from the measurements of the grain boundary composition in a (Mo,P)-low alloy steel with rather weak temperature dependence that may introduce a large error. From this point of view, the agreement of these data within the above scatters is remarkable. The experimental and predicted values for *nickel* differ substantially. In this case too, the value of ΔG_{Ni}^0 was determined from measurements of the composition of the grain boundaries in a complex ternary Fe–Ni–Sb alloy, which exhibits strong attractive interaction between nickel and antimony and thus, it is questionable whether the experimental value really represents ΔG_{Ni}^0.

Among the interstitially segregating elements, an excellent agreement between the predicted and experimental values was often achieved namely for *boron, phosphorus, sulphur* and *tin*. The value of $\Delta H_P^0 = -50\,\text{kJ/mol}$ determined assuming $\Delta S_P^0 = 0$ also represents de facto the value of ΔG_P^0. Some values of the enthalpy and entropy of phosphorus segregation given in Table 5.4, which differ substantially from the prediction, were determined from AES measurements in polycrystalline α-iron and ferritic steels and – as seen from Fig. 5.30 – they fit very well with the linear dependence between ΔH_P^0 and ΔS_P^0. It is highly probable that the sets of

Table 5.4 Predicted and experimental characteristics of grain boundary segregation in various α-iron-based binary systems

I	Prediction					Experiment					Ref.
	ΔH_I^0	ΔS_I^0	T	ΔG_I^0	X_I	X_I^Φ	X_I^Φ	ΔG_I^0	ΔH_I^0	ΔS_I^0	
Al	**−13**	**−9**	1,073	**−3.3**				**−3.4**	**−12**	**−8**	[587]
B	−76	−26	673	−58.5	0.04	**5.4**	**4**				[227]
C	**−50**	**+2**							**(−80**	**0)**	[588]
									(−37.7	**+43.2)**	[354]
									(−57	**+21.5)**	[589]
									(−79	**−13)**	[396]
Cr	**−13**	**−9**	773	**−6.0**				**−4.9**	**−8**	**−4**	[587]
Mo	−28	−25	773	**−8.7**				**−12 to −8.8**			[497]
			853	**−6.7**				**−20.0**			[590]
Ni	−20	−16	823	**−6.8**				**−14.4**			[418]
P	**−32**	**+22**							**−34.3**	**+21.5**	[328]
									−32	**+22**	[552]
									(−50	**0)**	[588]
									−21.2	**+37.3**	[355]
									−22	**+28**	[329]
									(−38	**0)**	[343]
			773	**−48.8**				**−44 to −33.5**			[497]
			853	**−50.6**				**−50**			[590]
S	−68	−17	823	**−54.0**	0.0035	**8.6**	**6.1**	**−51.5**			[381]
Sb	**−30**	**+24**							**(−19**	**+28)**	[335]
									−23	**+37**	[338]
									(−13	**−)**	[396]
			823	**−49.8**				**−32.7**			[397]
Si	−16	−12	823	**−7.0**	3	**7.0**	**10.3**	**−9.0**			[395]
			873	**−8.2**	4	**8.0**	**8.0**	**−5.3**			[591]
Sn	**−24**	**+30**	823	**−48.8**				**−44.0**	**−13.0**	**+45**	[592]
								−50.0	**−22.5**	**+26.1**	[593]
								−45.3	**−13.1**	**+39.1**	[593]

Concentrations in at.%, temperature in K. ΔG_I^0 and ΔH_I^0 in kJ/mol, ΔS_I^0 in J/(mol K). The data in bold are to be compared [375]. The data in bracket evidently represent the values of ΔG_I, ΔH_I and ΔS_I and cannot be directly compared with the values of ΔG_I^0, ΔH_I^0 and ΔS_I^0

thermodynamic functions [329,355] can be attributed to "less general" grain boundaries characterised by lower absolute values of the segregation enthalpy and higher entropy values. Only the values $\Delta H_P = -38$ kJ/mol and $\Delta S_P = 0$ [343] do not fit with the linear dependence although the value of ΔH_P is quite close to the predicted one. This is probably due to a specific way of determination of ΔH_P^0 (the authors used only the maximum values of X_I^Φ at each temperature for determination of the thermodynamic parameters of segregation [343]) that can be misleading, as discussed elsewhere [342]. The predicted and experimental values of ΔH_{Sb}^0 and ΔS_{Sb}^0 fit well with the compensation effect although a larger difference is apparent between these sets of the data. Similarly to phosphorus, this difference can be explained by measuring "less general" grain boundaries on the fracture surface

of polycrystals. The value $\Delta G^0_{Sb}(823\,K) = -32.7\,kJ/mol$ was determined from the measurements in a ternary Fe–Ni–Sb system by correcting for the excess contribution caused by attractive interaction between nickel and antimony according to the Guttmann procedure [416]. It is remarkable that this value is rather close to the predicted segregation enthalpy, $\Delta H^0_{Sb} = -30\,kJ/mol$.

Comparison of the predicted and experimental data marginally differs in case of *carbon*. As mentioned in Chap. 3, the determination of the thermodynamic functions from AES measurements of carbon grain boundary concentration is very complicated for several reasons. First, due to the ductilising effect of carbon on grain boundary brittle fracture, its interfacial segregation is often studied in a multi-component system containing an embrittling element and – similarly to the Fe–Ni–Sb system – the interaction effects between carbon and other solutes should be then considered. Second, carbide precipitation may occur in the bulk causing a substantial reduction of the concentrations of the solved carbon and other elements in α-iron solid solution. Last but not least, progressing contamination of the fracture surface by carbon from the residual gas atmosphere in the apparatus during the study may increase the carbon peak height measured by AES [594]. Probably, a combined effect of all these sources affects the quantification of AES spectra and is the origin of the discrepancies between predicted and experimental data for carbon (Table 5.4). Let us stress one important fact: There are clear differences of more than 40 kJ/mol in the experimental values of the enthalpy and of more than 50 J/(mol K) in the entropy reported by individual sources [354, 395, 588, 589] (Table 5.4). We can well assume that the analysed in situ fractured grain boundaries were general. In this case, very similar experimental values of ΔH^0_C and ΔS^0_C should be expected [94], as evident from the measurements on individual grain boundaries of different character, i.e. special, vicinal and general in model bicrystals [94]: The respective differences are 20 kJ/mol in enthalpy and 17 J/(mol K) in entropy for all grain boundaries while only 6 kJ/mol and 7 J/(mol K), respectively, for the general grain boundaries (cf. Fig. 5.30 and Appendix A). This suggests that the values of the thermodynamic functions [354, 395, 588, 589] represent a kind of ΔH^{eff}_{seg} and ΔS^{eff}_{seg} albeit not ΔH^0_C and ΔS^0_C.

In majority of cases, there is a very good agreement within ±5 kJ/mol and ±5 J/(mol K) for ΔH^0_I and ΔS^0_I, respectively: these limits are comparable with experimental uncertainties of measured values of segregation of any solute at general grain boundaries in α-iron and ferritic steels. Some discrepancies can be well explained on basis of complexity of the measurements of grain boundary segregation and of the systems studied. The above-mentioned remarkable agreement strongly supports the proposed prediction method, which is easy and straightforward. It was also shown that this method can predict chemical composition of low-alloy steels [375] as well as cast irons [17, 595] with fairly high precision. Let us mention that the equilibrium composition of ferrite solid solution has to be considered in case of these complex iron systems instead the nominal composition of the alloy: The solutes bound in precipitates are not allowable for segregation. This is very important mainly in case of carbon, whose concentration in solid solution is substantially reduced by precipitation [17, 375, 595].

5.7.2 Model of Wynblatt and Shi

Another approach to predict grain boundary segregation was proposed by Wynblatt and Shi [596]. Their model is based on the regular solution formalism of interfacial segregation [313, 324, 325]. The energy of the two adjoining crystals is described in terms of the nearest neighbour bonds. Each crystal consists of atoms located on the lattice points of (*hkl*) plane which terminates at the grain boundary so that no structural relaxations are permitted. In general, different (*hkl*) planes can meet at the grain boundary. They can be distinguished as $(hkl)_1$ and $(hkl)_2$ in respect to the two grains. The grains will be mutually rotated by a twist angle, ϕ, about the grain boundary normal. The five grain boundary DOFs are then used to define each of the two terminating (*hkl*) planes and the twist angle. Let us choose the description in which the indices of the terminating planes are $h \geq k \geq l$. The (*hkl*) planes in each crystal are denoted by index i, where $i = 1$ for the grain boundary plane. The second index, j, identifies the distance of the plane from plane i. The maximum value of j is denoted as $J_{\max}$, which represents the farthest plane containing nearest neighbours of the atoms in the ith plane. In fcc crystals $J_{\max} = \delta(h + k)$, where $\delta = 1/2$ if all h, k, l, are odd, and $\delta = 1$ for mixed h, k, l. The arrangement and the indices i and j are schematically shown in Fig. 5.33. Let us assume a fcc binary substitution solid solution A–B in which the solute is the component B. The composition of the ith atomic plane on one side of the grain boundary is given by (4.38). If the value of the segregation entropy is neglected, the Gibbs energy of segregation, ΔG_B^i, is replaced by the enthalpy of segregation, ΔH_B^i [596]. ΔH_B^i includes both the nearest neighbour bond as well as the elastic strain energy terms. In context of a nearest neighbour bond model, the relative locations of atoms across a grain boundary are

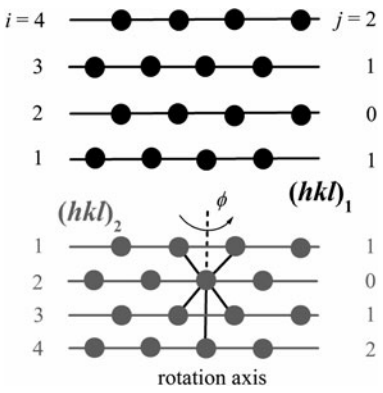

Fig. 5.33 Grain boundary between two crystals terminated by crystallographic planes $(hkl)_1$ and $(hkl)_2$, which are twisted by an angle ϕ about the grain boundary normal. The indices i number the planes away from the grain boundary plane. The indices j are illustrated here for the planes $i = 2$. A dangling bond from an atom in plane $i = 2$ is shown as a *dashed line*. Dangling bonds are reconnected to the other side of the grain boundary with probability P (see text) (according to [596])

not compatible with the nearest neighbour distances. Certain fraction of the dangling bonds of the atoms on one side of the grain boundary will be reconnected to the atoms on its other side. The fraction of the bonds reconnected to the other side of the grain boundary is given by a parameter, P, which depends on the Miller indices of the both boundary planes and on the twist angle ϕ [596].

The segregation enthalpy of the ith atom plane ($i \leq J_{\max}$) is given by

$$\Delta H_{\mathrm{B}}^{i} = 2\omega \left[\begin{array}{l} ZX - Z^{i}X^{i} - \sum\limits_{j=1}^{J_{\max}} Z^{j}X^{i+j} - \sum\limits_{j=1}^{i-1} Z^{j}X^{i-j} \\ -P \sum\limits_{j=1}^{J_{\max}} Z^{j}X' - \dfrac{1}{2}(1-P) \sum\limits_{j=1}^{J_{\max}} Z^{j} \end{array} \right]$$
$$-\frac{1}{2}(1-P)(\varepsilon_{\mathrm{BB}} - \varepsilon_{\mathrm{AA}}) \sum_{j=1}^{J_{\max}} Z^{j} - \Delta E_{\mathrm{el}}^{i} \tag{5.44}$$

and

$$\Delta H_{\mathrm{B}}^{i} = 2\omega \left[ZX - Z^{i}X^{i} - \sum_{j=1}^{J_{\max}} Z^{j}(X^{i+j} + X^{i-j}) \right] - \Delta E_{\mathrm{el}}^{i} \tag{5.45}$$

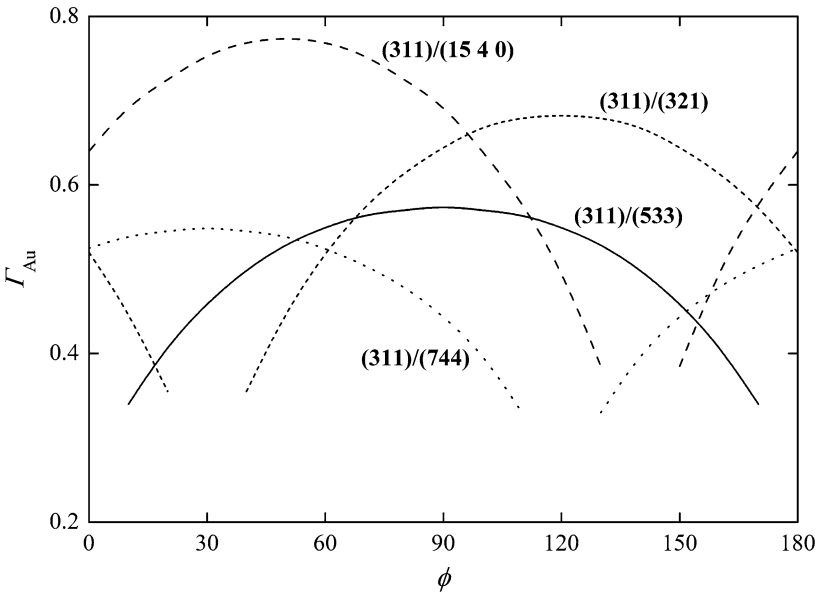

Fig. 5.34 Prediction of gold concentration at selected twist grain boundaries, terminated by a (311) plane on one side, as a function of the twist angle ϕ for a Pt–1at%Au alloy at 1,000 K (according to [597])

$X' = \sum_{i,j=1}^{J_{\max}} Z^j X^i / \sum_{i,j=1}^{J_{\max}} Z^j$. The equation for the determination of the composition of a plane i according to (5.44) or (5.45) in combination with (4.38) must be solved by iterative numerical methods [597].

Model of Wynblatt and Shi was applied to predict the composition of individual grain boundaries formed by the (311) plane on one side and by different (*hkl*) planes on the other side in a Pt–1at.%Au system at 1,000 K. In addition, the twist rotation by angle ϕ about the grain boundary normal was considered (Fig. 5.34). The results exhibit anisotropy of the gold segregation at the grain boundaries that is characterised by variations of the gold concentration approximately by factor three. A more pronounced anisotropy could be expected at lower temperatures or by considering a wider spectrum of the grain boundaries. The model also predicts the composition profiles across the interface. In an ideal solution, the composition on one side of the grain boundary depends only on its orientation and is independent of the orientation of the other side at the interface because no interaction occurs. In a real system, the degree of interaction will increase with increasing concentration and therefore, the interaction across the grain boundary is more effective [596, 597].